

This article was originally published in a journal published by Elsevier, and the attached copy is provided by Elsevier for the author's benefit and for the benefit of the author's institution, for non-commercial research and educational use including without limitation use in instruction at your institution, sending it to specific colleagues that you know, and providing a copy to your institution's administrator.

All other uses, reproduction and distribution, including without limitation commercial reprints, selling or licensing copies or access, or posting on open internet sites, your personal or institution's website or repository, are prohibited. For exceptions, permission may be sought for such use through Elsevier's permissions site at:

<http://www.elsevier.com/locate/permissionusematerial>

Deposition and re-entrainment dynamics of microbes and non-biological colloids during non-perturbed transport in porous media in the presence of an energy barrier to deposition

William P. Johnson ^{*}, Xiqing Li, Shoeleh Assemi

Department of Geology and Geophysics, University of Utah, 135 South 1460 East, Salt Lake City, UT 84112-0111, United States

Received 12 April 2005; received in revised form 27 October 2005; accepted 5 May 2006

Available online 12 September 2006

Abstract

This paper examines the non-perturbed deposition and re-entrainment dynamics of biological and non-biological colloids in porous media in the presence of an energy barrier to deposition at the grain surface. Deposition and re-entrainment rate coefficients were determined from numerical simulation of breakthrough–elution behavior and the profiles of retained colloids. We present composite trends from original and previously published data for biological and non-biological colloids which demonstrate that hydrodynamic drag mitigates deposition and drives re-entrainment of both biological and non-biological colloids in the presence of an energy barrier under non-perturbed conditions. Original data is presented for two sizes of colloids (1.1 and 5.7 μm microspheres) under a variety of ionic strength and fluid velocity conditions to examine the torque balance governing re-entrainment of colloids attached to the grain surfaces. The analysis indicates that in the presence of an energy barrier to deposition, hydrodynamic drag may influence deposition and re-entrainment of colloids associated directly with the grain surface via primary energy minima. However, the hydrodynamic field would also be expected to influence deposition and re-entrainment of colloids associated with the surface via secondary energy minima. Hence, the observed influences of fluid velocity are consistent with colloid association via either mechanism. These results call for the development of colloid transport theories that explicitly account for the influence of the hydrodynamic field at the grain surface.

© 2006 Elsevier Ltd. All rights reserved.

Keywords: Transport; Groundwater; Bacteria; Colloid; Detachment; Re-entrainment; Fluid drag

1. Introduction

Biological and non-biological colloid transport behaviors in porous media are controlled by a deceptively short list of processes: advection, dispersion, deposition and re-entrainment, which are governed by complex characteristics of the subsurface and the colloid. Advection and dispersion are dominantly controlled by macro- to micro-scale physical characteristics of porous media, specifically, by permeability and permeability contrasts in the subsurface [20,24,4,130,56,145,91,101,154,76]. Deposition and re-entrainment are controlled by a larger set of characteristics of the system that range from the micro- to the nano-

scale, that include both physical and chemical characteristics [11,119], and that shift in response to perturbations in groundwater flow and solution chemistry [44,117,109,110,79,111].

Biological colloids (e.g. viruses, bacteria, and protozoa) and non-biological colloids (e.g. microspheres and mineral colloids) differ fundamentally in terms of potential physiological controls on their transport in porous media. For example, the attachment and detachment behaviors of microbes may vary due to physiologic processes or features such as growth [55,46,92], starvation [55], polymer secretion [94,73], and the presence of appendages, e.g. flagella [23,143,144]. Even when these differences are neutralized (e.g. by starvation); biological and non-biological colloids may differ in terms of the contribution of polymeric materials to their surface characteristics [98,99,74,90,22,58,141,

^{*} Corresponding author. Tel.: +1 801 5815033; fax: +1 801 5817065.
E-mail address: wjohnson@mines.utah.edu (W.P. Johnson).

Nomenclature

REV	representative elementary volume ($L_{\text{water+grains}}^3$)	h_p	the pore length (L)
M	mass	v_{colloid}	fluid velocity at the center point of the retained colloid ($L_{\text{REV}}t^{-1}$)
L	length	N_{pore}	number of pores in the column cross section
t	time	F_A	adhesion force (MLt^{-2})
k_f	colloid deposition rate coefficient (t^{-1})	l_x	lever arm (L)
d_c	porous media grain (collector) diameter (L)	T_A	adhesive torque (ML^2t^{-2})
θ	is the volumetric water content of the saturated porous media ($L_{\text{water}}^3L_{\text{REV}}^{-3}$)	a_o	radius of colloid-surface contact (L)
v	fluid velocity ($L_{\text{REV}}t^{-1}$)	K	elastic interaction constant ($ML^{-1}t^{-2}$)
η	collector efficiency (collisions/approaches)	E	Young's modulus ($ML^{-1}t^{-2}$)
α	deposition efficiency (attachments/collisions)	ν	Poisson ratio (dimensionless)
C	number concentration of colloids in aqueous phase ($\#-L_{\text{water}}^{-3}$)	D	dispersion coefficient of the colloids (L^2t^{-1})
C_0	number concentration of colloids in aqueous phase at source ($\#-L_{\text{water}}^{-3}$)	ρ_b	bulk density of porous media ($M_{\text{sed}}L_{\text{REV}}^{-3}$)
x	distance from source (L)	k_r	re-entrainment rate coefficient (t^{-1})
k	Boltzmann's constant ($1.38E-23 ML^{-2}t^{-2}K$)	S_r	number concentration of retained colloids that are reversibly retained ($\#-M_{\text{sed}}^{-1}$)
T	temperature (298.2 K)	S	total number concentration of retained colloids ($\#-M_{\text{sed}}^{-1}$)
a_{colloid}	radius of colloid (L)	f_{ir}	fraction of retained colloids that are irreversibly retained
μ	dynamic viscosity of the aqueous phase (Mt^{-2})	A_{11}, A_{22} and A_{33}	individual Hamaker constants for polystyrene, water, and glass, respectively (ML^2t^{-2})
$F_{\text{hydrodynamic}}$	hydrodynamic drag force (MLt^{-2})	ΔG	total energy of colloid-surface interaction (electric double layer and van der Waals components) at a given separation distance (ML^2t^{-2})
$T_{\text{hydrodynamic}}$	hydrodynamic torque (ML^2t^{-2})		
d_z	diameter of pore (L)		
z	distance along the pore (L)		
d_{con}	equivalent diameter of the pore constriction (L)		
d_{max}	the maximum pore diameter (L)		

21,1,128]. Despite the prevalence of differences between biological and non-biological colloids, their transport behaviors in porous media share important similarities, such as:

- (1) They undergo deposition in porous media even when their interaction energies with the porous media indicate that direct attachment to the surface should be prevented by a formidable energy barrier.
- (2) Their retained profiles on porous media deviate from the log-linear shape expected from classic filtration theory if an energy barrier to deposition is present.
- (3) Their deposition rates decrease with increasing fluid velocity, in opposition to expectations from existing theory.
- (4) They undergo slow re-entrainment from the porous media even in the absence of perturbations in solution chemistry or flow.

These common attributes (further substantiated below) of the deposition behaviors of biological and non-biological colloids indicate processes underlying deposition that occur independently of the characteristics of the particular colloid. The purpose of this paper is to demonstrate that even in the absence of permeability contrasts and perturbations in ground water flow and solution chemistry, the

transport behaviors of biological and non-biological colloids in porous media are significantly influenced by hydrodynamic forces that mitigate deposition to, and drive re-entrainment from, porous media. These hydrodynamic influences are currently absent from existing colloid transport models, yet they are here demonstrated to be significant for both biological and non-biological colloids even in the absence of flow perturbations, in the presence of an energy barrier to deposition, as is prevalent under environmental conditions.

2. Background

2.1. Deposition in the presence of an energy barrier

Interaction forces between colloids and porous media are classically estimated based on the respective contributions from electric double layer and van der Waals interaction energies [38,142,137,136]. Surfaces of environmental colloids (biological and non-biological) and porous media tend to display overall like charge (negative), yielding overall repulsive electric double layer energies between them. The overall negative surface charge emanates from acidic functional groups, which dominate the surfaces of biological colloids and the surfaces of silicate mineral grains under most environmentally relevant groundwater conditions

(e.g. pH 6–9) [35,127]. However, some of the minor mineral phases in porous media such as iron oxides may display positive surface charge at environmental pH conditions. One can characterize the bulk of subsurface media as being negatively charged, but with varying extents of surface charge heterogeneity arising from mineral phases such as iron oxides [123,122,27,64]. The prevalence of natural organic matter in the environment results in masking of positive surface charges by adsorbed natural organic matter, which carries negative charge derived from carboxylic and phenolic functional groups [126,127,35]. The overall negative surface charge on colloids and porous media surfaces in environmental systems yields an electric double layer energy barrier to deposition at colloid-surface separation distances ranging from a few to more than one hundred nm, depending on system conditions.

Colloid deposition is mediated not only by colloid-surface interaction energies, but also by the likelihood of colloid collision with porous media grain surfaces. This probability of collision is estimable on the basis of the physical properties of the system, as enveloped in filtration theory [151,105,83]. The probability of collision is estimated from an easily implemented expression that correlates readily measured physical parameters to numerical simulations accounting for advection of colloids on streamlines that will result in collision with grain surfaces, as well as colloid crossing of streamlines via diffusion and gravitational settling [131,93]. Filtration theory is a highly useful construct that has been demonstrated to predict accurately the probability of colloid collision with porous media surfaces in ideal systems (e.g. lacking an energy barrier to deposition).

The probability of colloid collision with porous media grain surfaces (collector efficiency, η) yields a colloid deposition rate coefficient (k_f):

$$k_f = \frac{3}{2} \frac{(1 - \theta)}{d_c} v \eta \quad (1)$$

where θ is the porosity of the porous media, d_c is the porous media grain diameter, and v is the fluid velocity. In an ideal system lacking an energy barrier, the colloid deposition rate coefficient accurately predicts a log-linear decrease in the concentration (C) of suspended (and retained) colloids as a function of distance (x) from the source:

$$\ln \frac{C}{C_0} = -\frac{k_f}{v} x \quad (2)$$

where C_0 is the concentration at the source. In the presence of a significant energy barrier to deposition (e.g. >10 kT), the explicit numerical models of colloid deposition predict no colloid deposition [e.g. 41]. However, the prevalence of colloid deposition in environmental systems despite the presence of significant energy barriers to deposition is well demonstrated; for example, by the general success of filtration as a water treatment technology and by the generally higher quality of ground water relative to surface water.

To quantify deposition in the presence relative to the absence of an energy barrier to deposition, an additional

parameter accounting for the probability of deposition upon collision (deposition efficiency, α) is multiplied against the right hand side of Eq. (1). Reconciliation of theory to practice (deposition despite a large estimated energy barrier) has been advanced by invoking a variety of processes that have not yet been comprehensively incorporated into theory: (1) localized nanoscale patches of attractive surface charge [41,122,123,64]; (2) surface roughness [11,119]; (3) deposition at grain-grain contacts [29], (4) straining [17,16,133]; and (5) deposition in the weakly attractive energy minimum (secondary energy minimum) outboard (at greater separation distances) from the interaction energy barrier [52,51].

2.2. Deviation of retained colloid profiles from classic filtration theory

Colloid deposition in the presence of an energy barrier yields profiles of retained colloids that deviate from the log-linear behavior expected from classic filtration theory (Eq. (2)). This result was originally observed in the bacterial transport literature, and was ascribed to heterogeneity among the bacterial population [57,3,37,7,120,12,13,153]; the practical implication being that classic filtration theory under-estimates microbial transport distances, since the colloidal population becomes less sticky with increasing distance of transport. This observation was quickly extended to virus transport [5,103,116,106], and was demonstrated in a recent compilation of field data [100], where the observed “filtration factors” decreased greatly over transport distances ranging from tens to hundreds of meters from the source.

Recently, deviation from classic filtration theory has been recognized as a general aspect of colloid filtration in the presence of an energy barrier to deposition [81,132,66]. The retained colloid profiles obtained in the presence of an energy barrier to deposition indicate that the deposition rate coefficient is spatially variable, typically showing apparent decreases in the deposition rate coefficient with increasing transport distance. However, non-monotonic variations in the deposition rate coefficient with transport distance are also observed, e.g. apparent increases in the deposition rate coefficient with transport distance at relatively short distances, followed by apparent decreases in the deposition rate coefficient with increasing transport distance [80,129]. The energy barrier to deposition that drives deviation from classic filtration theory is not necessarily strictly electrostatic or osmotic in origin, but rather may result from steric interactions [128]. Additionally, physical straining may contribute to deviation from log-linear retained colloid profiles under some circumstances [17,16,15].

2.3. Re-entrainment in the absence of perturbations

Another important aspect of colloidal transport in the presence of an energy barrier to deposition is the slow

steady re-entrainment of colloids, sometimes referred to as extended tailing, which is observed ubiquitously for both biological and non-biological colloids in laboratory and field contexts. Extended tailing has been observed in laboratory experiments examining transport of carboxylated latex microspheres [149,95,58,28], natural mineral colloids [49], bacteria [44,61,125,82,85,68], and protists [55,53]. Extended tailing has also been well-observed in field transport of natural mineral colloids [84], bacteria [57,117,55,153], and bacteriophage [111,36,116]. Since extended tailing is observed in the absence of perturbations in solution chemistry or flow, the observed slow re-entrainment likely represents shifts in the microscale environment of the retained colloid.

Re-entrainment often is dwarfed by deposition, and so can often be neglected relative to other processes governing net deposition. The significance of re-entrainment is that it may potentially increase the transport distance of colloids over the long term (years), as demonstrated in simulations examining colloid transport using deposition and re-entrainment rate coefficients estimated from a field study of bacterial transport [153]. In the short term, however, re-entrainment provides insight into the mechanism of deposition. In experiments examining deposition of polystyrene latex microspheres, deposition in the absence of an energy barrier resulted in negligible re-entrainment; whereas deposition in the presence of an energy barrier resulted in significant re-entrainment (Li et al., 2005). In some contexts, deposition is highly reversible, e.g. recent laboratory experiments demonstrated re-entrainment-driven translation of the center of mass of retained bacteria in glass beads over distances of several cm in a few hours [129]. Determining the generality of this phenomenon requires examination of the retained profiles of other bacterial strains.

2.4. Re-entrainment evaluated via torque balance

In the case where a colloid is attached directly to the collector surface (i.e. via primary minimum), the process of re-entrainment can be referred to more specifically as detachment. Most colloid detachment studies performed to date concern detachment in response to macroscopic perturbations in flow or solution chemistry [109,110,75,8], resulting in greater understanding of the balance between hydrodynamic and adhesion forces that drive and resist detachment, respectively [62,33,8]. Since rolling is the dominant mechanism of incipient detachment from collector surfaces [62,118,33,152], detachment is governed by the balance between the hydrodynamic and adhesive torques on an attached particle.

The hydrodynamic drag force experienced by an attached colloid is related to the fluid velocity (v), the radius of the colloid (a_{colloid}), and the viscosity of the fluid (μ) [45,96,118], where the leading coefficient below (1.7) results from wall effects at close proximity to the grain surface:

$$F_{\text{hydrodynamic}} = (1.7)6\pi\mu a_{\text{colloid}}v \quad (3)$$

The hydrodynamic torque driving detachment is the product of the hydrodynamic force and the lever arm that causes the hydrodynamic force to act at an effective distance from the grain surface equal to $1.399a_{\text{colloid}}$ [118]:

$$T_{\text{hydrodynamic}} = 1.399a_{\text{colloid}}F_{\text{hydrodynamic}} \quad (4)$$

Most research has considered the balance of hydrodynamic and adhesive torques on an attached particle in simple shear systems where it is relatively easy to estimate fluid velocities. The fluid velocity at the center point of the retained colloid in porous media can be derived from a representative pore structure using constricted tube model [102,8], in which the pore space is comprised of a series of parabolic constrictions, the diameter (d_z) of which is a function of distance along the pore (z):

$$d_z = 2 \left\{ \frac{d_{\text{max}}}{2} + \left[4 \left(\frac{d_{\text{con}}}{2} - \frac{d_{\text{max}}}{2} \right) \left(0.5 - \frac{z}{h_p} \right)^2 \right] \right\} \quad (5)$$

where d_{con} is the equivalent diameter of the constriction ($=d_c/2.57$ [8]), d_{max} is the maximum pore diameter, and h_p is the pore length. The fluid velocity at the center point of the retained colloid can be determined as follows [8]:

$$v_{\text{colloid}} = \frac{Q/N_{\text{pore}}}{(\pi/4)d_z^2} \frac{4(d_z/2 - a_{\text{colloid}})}{(d_z/2)^2} \quad (6)$$

where Q is the volumetric flow rate in the porous media, N_{pore} is the number of pores in the column cross section.

The adhesive torque (T_A) is represented by the adhesion force (F_A) acting on a lever arm l_x :

$$T_A = F_A l_x \quad (7)$$

The lever arm is provided by the radius of colloid-surface contact (a_0), which results from deformation of the microsphere [71,146,70] or deformation of the grain surface. In our system, deformation of the grain surface is expected to be negligible compared to that of the microsphere since the Young's modulus of elasticity of glass, $6.9 \times 10^{10} \text{ N m}^{-2}$, is much greater than that of polystyrene, $0.28 \times 10^{10} \text{ N m}^{-2}$ [10]. Therefore, the microsphere will deform to yield a contact radius that is proportional to the adhesion force [71,63]:

$$a_0 = (4F_A a_{\text{colloid}}/K)^{1/3} \quad (8)$$

where K is the elastic interaction constant, which is calculated from the Poisson ratio (ν) and the Young's modulus (E) as follows:

$$K = \frac{4}{3} \left\{ \frac{1 - \nu_{\text{colloid}}^2}{E_{\text{colloid}}} + \frac{1 - \nu_{\text{glass}}^2}{E_{\text{glass}}} \right\}^{-1} \quad (9)$$

For the glass-polystyrene system used here, K was calculated as $4.0 \times 10^9 \text{ N m}^{-2}$ using published values of the Poisson ratio and Young's Modulus for these materials [10].

3. Methods

3.1. Experimental conditions

The microspheres used in these porous media experiments were spherical fluorescent carboxylate-modified polystyrene latex microspheres of two sizes (1.1 and 5.7 μm in diameter). The 1.1 μm microsphere stock suspension (Molecular Probes, Inc., Eugene, OR) was used as received with a particle concentration of $2.7 \times 10^{10} \text{ mL}^{-1}$, and a NaN_3 concentration of 2 mM. Prior to injection, an aliquot of the 1.1 μm stock suspension was diluted by a factor of 2000 in salt solution with the desired ionic strength ($C_o = 1.35 \times 10^7$ particles mL^{-1}). The 5.7 μm microsphere suspension (Bangs Laboratories, Inc., Fishers, IN) was used as received with 0.01% of Tween-20, 2 mM of NaN_3 , and 9.4×10^7 particles mL^{-1} . Prior to injection, the stock 5.7 μm microsphere suspension was diluted in salt solution by a factor of 100 ($C_o = 9.4 \times 10^5$ particles mL^{-1}).

Spherical soda lime glass beads (Cataphote Inc., Jackson, MS) were used as the porous media. The glass beads were dry-sieved using 40 and 50 mesh USA standard testing sieves (The W.S Tyler Company, Mentor, OH), resulting in glass bead sizes ranging from 300 to 417 μm . Following dry sieving, wet sieving was also performed using the same sieves in deionized water, as suggested by Brown et al. [19]. In some of the replicate experiments, sediments that were not wet-sieved were used in order to examine the effect of wet sieving on microsphere transport. No significant differences were observed in the results regardless of sieving treatment under the ionic strength range examined in this study. The cleaning procedure of the glass beads was based on that used by Bergendahl et al. (1999). The glass beads were first rinsed sequentially with acetone and hexane and then soaked with concentrated HCl for about 12 h. After repeated rinsing with deionized water, the glass beads were soaked with 0.1 M NaOH for approximately 12 h, followed by repeated rinsing with ultra pure water (Millipore Corp. Bedford, MA) until the ionic strength was negligible relative to the experimental ionic strength, as determined using a conductivity meter (Conductance/TDS Model 72, Engineered Systems & Design, Newark, DE).

The cylindrical Plexiglass columns (20 cm in length and 3.81 cm in inner diameter) were dry-packed after the glass beads were dried at 105 $^\circ\text{C}$ and cooled. Packing was performed by adding glass beads in small increments (~ 2 cm) with mild vibration of the column. Two 60-mesh stainless steel screens (Gerard Daniel Worldwide, Hanover, PA) were placed at each end of the column. To spread the flow upon entry into the column, coarse sand (3.5 g, >30 mesh, cleaned as described above) was added to the top of the influent screen, forming a thin layer (2 mm) that was covered by another screen. The porosities of the packed glass beads (determined by mass and tracer breakthrough) were 0.37 and 0.39, respectively for the two batches of glass beads used.

The packed columns were purged with CO_2 for at least 30 min to remove air, and were then pre-equilibrated by salt solution with the desired ionic strength for six pore volumes. One pore volume was equal to 83 mL and 89 mL at the porosities of 0.37 and 0.39, respectively. After pre-equilibration, three pore volumes of microsphere suspension was injected, followed by seven pore volumes of salt solution (without microspheres) at the same ionic strength. During injection, the microsphere suspension reservoirs were sonicated for 1 min each hour to minimize aggregation, as verified by flow cytometric analyses. The ionic strengths of the pre-equilibration and the injection solutions were varied over a range from 0.001 to 0.02 M (NaCl), whereas the influent pH was measured to be 6.0 at all ionic strengths following equilibration with the atmosphere. The pH of the solution was allowed to vary in response to solution interaction with the glass beads, as described further in [129]. Effluent pH was approximately 9.3.

The flow rate was varied to produce pore water velocities ranging between 1 and 8 m day^{-1} . It should be noted that although the fluid velocities examined here are low relative to those typically examined in colloid transport studies, they are still somewhat high relative to velocities expected in some groundwater settings. As such they can be considered reflective of velocities encountered under natural gradient conditions in relatively coarse media (e.g. coarse sand or alluvial aquifers), or under forced gradient conditions (e.g. riverbank filtration systems).

The solutions were injected in up-flow mode using a syringe pump (Harvard Apparatus, Inc, Holliston, MA). During injection the syringes were refilled every 23 mL at a refill rate of 46 mL min^{-1} for flow rates between 1 and 4 m day^{-1} , and at a refill rate of 60 mL min^{-1} at the 8 m day^{-1} flow rate.

The 5.7 μm microspheres were subject to a minor amount of settling within the syringe during injection by the syringe pump. A study of the microsphere concentration exiting the syringe showed that this concentration was a factor of 0.88, 0.93, 0.97 relative to the concentration in the periodically sonicated feed reservoir at flow rates of 2, 4, and 8 m day^{-1} , respectively. This factor was applied to the influent concentration prior to calculation of normalized effluent microsphere concentrations and mass balances.

Column effluent samples were collected in 5 mL polystyrene tubes (Becton Dickinson & Co., Franklin Lakes, NJ) using a fraction collector (CF-1, Spectrum Chromatography, Houston, TX). Following the experiment, the sediment was dissected into ten 2 cm-long segments, as the sediment was released from the column under the gravity. Attached colloids were recovered by placing sediment segments (2 cm) into specified volumes of Milli-Q water and sonicating for 1 min. These specified volumes were 200 mL for the first two segments at the column inlet, 100 mL for the third segment, and 25 mL for all subsequent segments.

Aqueous effluent samples, and supernatant samples from recovery of attached microspheres, were analyzed using flow cytometry (BD FACScan, Becton Dickinson & Co., Franklin Lakes, NJ). The samples were run using a flow rate of $12 \mu\text{L}\cdot\text{min}^{-1}$ at an excitation wavelength of 488 nm and were counted for 1 min. Conversion of “event” counts on the flow cytometer into microsphere concentrations was made using a calibration curve based on serial dilutions of microsphere suspensions of known concentration. The R^2 of the log–log calibration curves were consistently greater than 0.99. The flow cytometer was able to track aggregation of microspheres as doublets and triplets based on their respective light scattering properties.

The area under the breakthrough–elution curve was integrated to yield the percentage of microspheres exiting the column. The percent of injected microspheres recovered from the sediment was determined by summing the number of microspheres recovered from all segments of the sediment and dividing by the total number injected. The overall recovery (mass balance) of microspheres was determined by summing the percentages of microspheres that exited and that were retained in the column.

3.2. Modeling

The transport of the microspheres was modeled using an advection–dispersion equation that includes deposition from, and re-entrainment to, the aqueous phase:

$$\frac{\partial C}{\partial t} = -v \frac{\partial C}{\partial x} + D \frac{\partial^2 C}{\partial x^2} - k_f C + \frac{\rho_b}{\theta} k_r S_r \quad (10)$$

where C is the microsphere concentration in aqueous phase (particles per unit volume of fluid), t the travel time, x the travel distance, v the fluid velocity, D the dispersion coefficient of the colloids, θ the porosity, ρ_b the bulk density of sediment, k_f and k_r are rate coefficients of microsphere deposition to and re-entrainment from solid phase respectively. S_r is the reversibly retained microsphere concentration on the solid phase (particles per unit mass of sediment) and can be further expressed as

$$S_r = S(1 - f_{ir}) \quad (11)$$

$$\frac{\partial S}{\partial t} = \frac{\theta}{\rho_b} k_f C - k_r S_r \quad (12)$$

where S is the total removed concentration and f_{ir} is the fraction of irreversibly deposited colloids. A one-dimensional discrete random-walk particle-tracking model was used to simulate microsphere transport (Eqs. (10)–(12)).

The representation of k_f , k_r , and f_{ir} in the particle model is described in detail elsewhere [153,154,115,81]. It is important to note that the probabilistic approach used in the particle-tracking model decouples the parameters k_f and f_{ir} , whereas this decoupling is not apparent (Eqs. (10)–(12)). Additionally in the equations as written in continuum form, results for experiments involving an energy barrier to deposition are typically better-represented using

a distribution of deposition rate coefficients (k_f) [81], Tufenkji et al. (2004b). Log-normal distributions of k_f values were also utilized in the simulations presented below, and were implemented in the manner described in detail in [81]. The single collector efficiency (η) in Eq. (1) can be calculated using the correlation equations developed by Rajgopalan and Tien (1979), and Tufenkji and Elimelech [131], abbreviated below as the R–T and T–E equations, respectively.

3.3. Atomic force microscopy measurements

The adhesion force was approximated by the pull-off force measured using atomic force microscopy (AFM) between a glass surface and the microspheres. The shortcomings of theory in explaining colloidal attachment–detachment behavior provides the basis for the emergence of atomic force microscopy (AFM) for direct measurement of interaction and adhesion energy force profiles between colloids and surfaces. In AFM, forces between the substrate and a colloidal probe can be measured in solution [39] and characterized. This method has been extensively used to characterize the forces between different minerals [39,139,54,140,60], and has more recently been utilized in studies of microbe–surface interaction [97,22,141,21].

The 1.1 and 5.7 μm microspheres were glued to the tips of V-shaped silicon-nitride cantilevers (Veeco, Santa Barbara, CA) using a micromanipulator and Loctite 325 adhesive and Loctite 7075 activator glue. For the 5.7 μm microsphere, the spring constant was determined as 0.10 N m^{-1} , using the Cleveland method [25]. The forces between the 5.7 μm microspheres and a glass slide were measured in a quartz fluid cell using a Nanoscope IIIa atomic force microscope (Veeco, Santa Barbara, CA). For the 1.1 μm microspheres, the spring constant of the cantilever was determined as 0.16 N m^{-1} using thermal noise [113]. The forces between the 1.1 μm microsphere and a glass slide were measured using a PicoPlus atomic force microscope (Molecular Imaging, Tempe, AZ). Measurements were made in a droplet of solution (200 μL) on the glass slide. Time of measurement was limited (e.g. 15–30 min) to avoid significant concentration of electrolyte by evaporation. The raw data (voltage versus deflection) was converted to force versus distance using force analysis software; AFM Analysis (University of Melbourne, Australia) and SPIP (Image Metrology, Denmark).

3.4. DLVO interaction energy profiles

In order to support interpretation of trends in deposition rate coefficients, the interaction energies as a function of separation distance between the 1.1- μm microsphere and the glass beads were calculated using DLVO theory. The electrophoretic mobilities of the microspheres and crushed glass beads were measured using a ZetaPALS Analyzer (Brookhaven Instruments, Holtsville, NY) and were converted to zeta potentials using the von Smoluchowski

approach [121]. The electric double layer repulsive interaction and retarded van der Waals attractive interaction were calculated based on approximate expressions developed by Gregory [47,48]. The decay length for the van der Waals interaction was 100 nm, and the Hamaker constant was 3.8×10^{-21} J for microsphere–water–glass system using the following equation:

$$A_{132} = (\sqrt{A_{11}} - \sqrt{A_{33}})(\sqrt{A_{22}} - \sqrt{A_{33}}) \quad (13)$$

where A_{11} , A_{22} and A_{33} are the individual Hamaker constants for polystyrene, water, and glass taken from the literature as 6.6×10^{-20} J, 3.70×10^{-20} J, and 6.34×10^{-20} J, respectively [63,9].

4. Results

4.1. Mass balances

Mass recoveries (total from effluent and sediment) were virtually all between 90% and 110%, with the vast majority showing between 95% and 105% recovery (Table 1). The excellent mass balance shows that the microspheres were detached by dilution into pure water, indicating that their mechanism of retention was eliminated either by disassembling the pore structure or by increasing the magnitude of colloid-collector electric double layer repulsion.

4.2. Electrokinetic potentials

The influence of ionic strength on the zeta potentials of the microspheres (pH 6.0) are presented in Fig. 1. The zeta potentials were consistently lower for the 5.7 μm microspheres relative to the 1.1 μm microspheres. The zeta potentials of both microspheres became less negative with increasing ionic strength due to compression of the electric double layer. The zeta potentials of the 5.7 μm microspheres decreased from about -50 to -10 mV, whereas

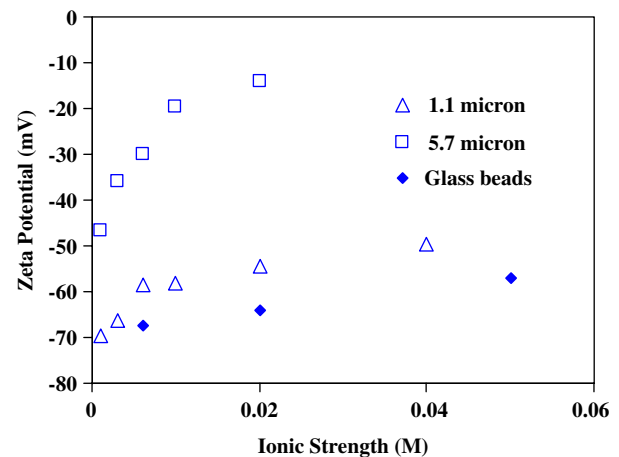


Fig. 1. Zeta potentials of the microspheres and crushed glass beads as a function of ionic strength.

the zeta potentials of the 1.1 μm microspheres decreased from -70 to -50 mV, over the ionic strength range from 0.0038 M to 0.05 M. The zeta potentials of the crushed glass beads ranged from -67.5 to -57.0 mV over this ionic strength range.

4.3. Breakthrough–elution curves and retained colloid profiles

The effluent breakthrough–elution curves (top row) and retained colloid profiles (bottom row) are shown in Figs. 2–5. Figs. 2 and 3 display the ionic strength series for the 1.1 μm and 5.7 μm microspheres, respectively. Figs. 4 and 5 display the fluid velocity series for the 1.1 μm and 5.7 μm microspheres, respectively. Error bars in the effluent breakthrough–elution curves and the attached profiles represent standard deviations from replicate experiments, with the number of replicates ranging between 1 and 4.

Table 1

Column experiment conditions, mass balances, and model parameters for simulations using the particle-tracking model

Conditions		Recovery		Distributed k_f				Single k_f				
Size (μm)	IS (M)	v (m day^{-1})	N	% Rec	% Sed	Mean k_f (h^{-1})	Std. dev. k_f	k_r (h^{-1})	f_{ir}	k_f (h^{-1})	k_r (h^{-1})	f_{ir}
1.1	0.001	4	3	98.9	2.85	0.56	5.9	0.34	0.31	0.050 ^a	0.26 ^a	0.69 ^a
1.1	0.006	4	1	99.1	17.1	2.1	11.9	0.33	0.50	0.15 ^a	0.33 ^a	0.74 ^a
1.1	0.01	4	2	96.6	34.4	5.8	18.9	0.27	0.73	0.39 ^a	0.23 ^a	0.92 ^a
1.1	0.02	4	4	109.5	67.2	6.7	17.8	0.25	0.94	0.71 ^a	0.25 ^a	0.98 ^a
1.1	0.02	2	1	89.9	65.7	39.0	43.9	0.16	0.77	0.63 ^a	0.11 ^a	0.96 ^a
1.1	0.02	8	2	97.8	21.0	5.4	18.4	1.0	0.70	0.48 ^a	0.38 ^a	0.96 ^a
5.7	0.001	4	1	100.0	5.5	1.37	9.25	1.0	0.15	0.09 ^a	0.48 ^a	0.5 ^a
5.7	0.006	4	3	104.5	15.8	7.85	24.6	1.2	0.1	0.2 ^a	0.5 ^a	0.5 ^a
5.7	0.01	4	3	107.2	34.1	11.0	28.5	0.70	0.27	0.32 ^a	0.4 ^a	0.7 ^a
5.7	0.02	4	3	111.9	71.7	37.5	44.1	0.61	0.27	0.93 ^a	0.3 ^a	0.8 ^a
5.7	0.02	2	1	97.6	92.1	21.7	27.8	0.4	0.4	1.5 ^a	0.2 ^a	0.75 ^a
5.7	0.02	8	2	110.6	53.4	27.0	40.9	1.21	0.3	1.15 ^a	0.52 ^a	0.85 ^a

“IS” indicates ionic strength (M NaCl), “Vel” indicates pore water velocity. “ N ” refers to the number of replicates. “% Rec” refers to average percent total injected microspheres recovered (from porous media and effluent) for the experimental condition. “% Sed” refers to average percent of microspheres on the porous media at the end of the experiment.

^a Refers to parameter values determined for condition std. dev. $k_f = 0$. Where std. dev. $k_f \neq 0$, k_f refers to mean.

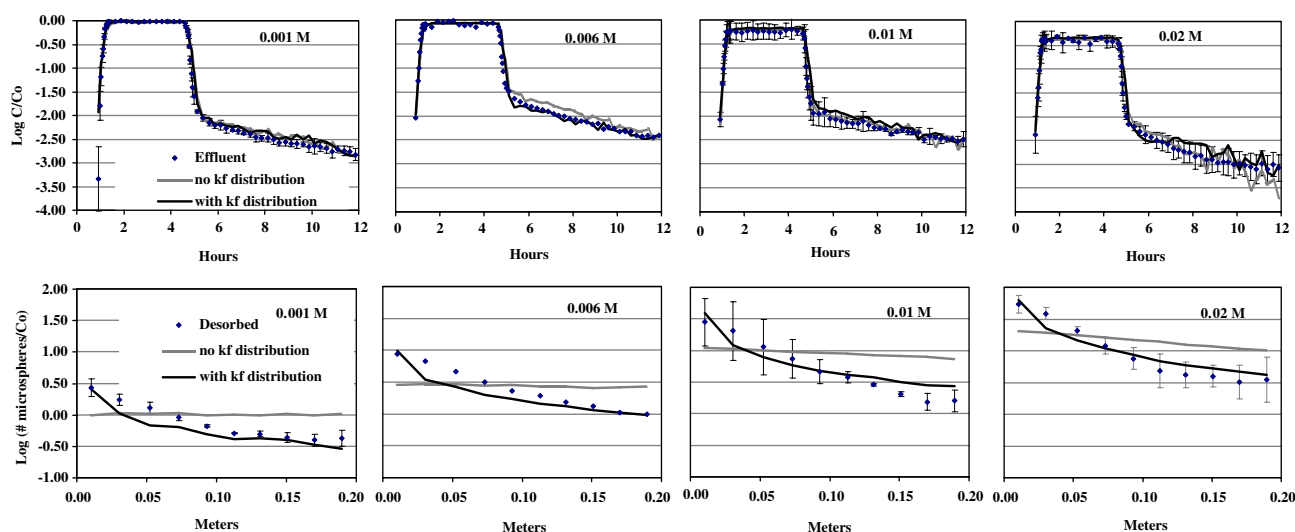


Fig. 2. Ionic strength series for 1.1- μm microspheres at velocity = 4 m day^{-1} , showing effluent breakthrough–elution curves (top), and attached profiles (bottom). Error bars represent standard deviations in results from replicate experiments ($n = 2\text{--}4$). Simulations using the particle transport model without an attachment rate (k_f) distribution (dashed line) are contrasted against those using an attachment rate (k_f) distribution (solid line).

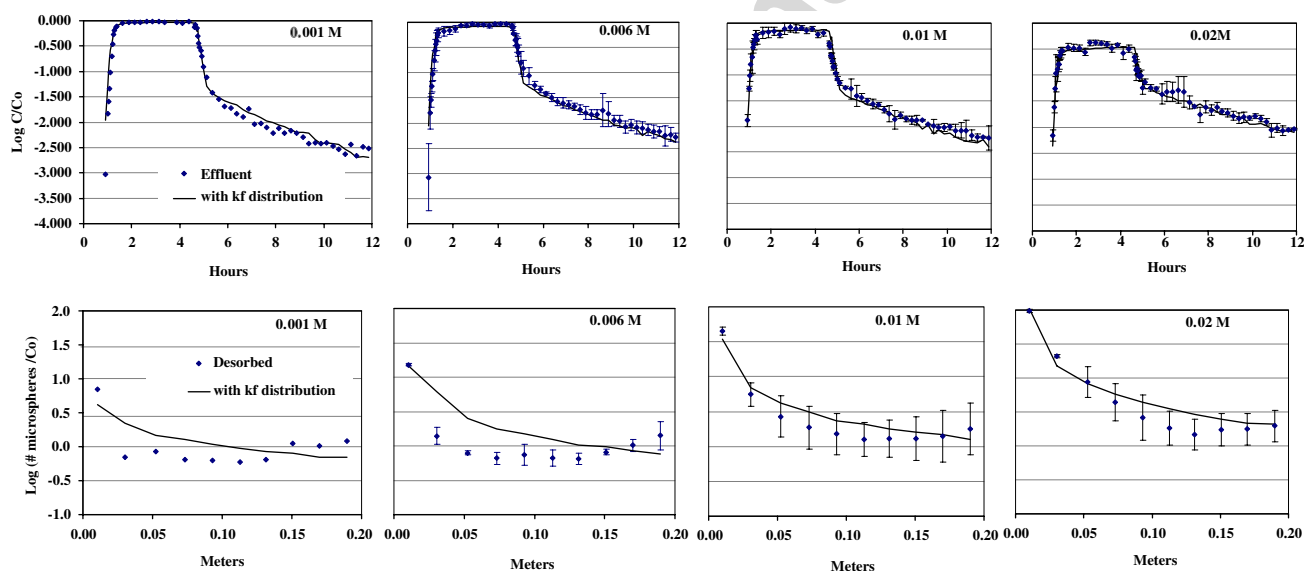


Fig. 3. Ionic strength series for 5.7- μm microspheres at velocity = 4 m day^{-1} , showing effluent breakthrough–elution curves (top), and attached profiles (bottom). Error bars represent standard deviations in results from replicate experiments ($n = 2\text{--}4$). Simulations are shown using the particle transport model with an attachment rate (k_f) distribution (solid line).

The particle transport model was able to simulate well the effluent data regardless of whether or not a distribution in attachment rates was used (Figs. 2–5). However, the attached profiles could not be simulated using a constant rate of attachment (no k_f distribution) (Fig. 2, bottom). The distributed deposition rate coefficient model provided good simulations of the effluent and retained microsphere concentrations using a single set of parameters, except for the 5.7 μm microspheres at the low ionic strength conditions (Fig. 3, bottom). Previous papers have explored the origin of these “hyper-exponential” retained colloid profiles (e.g. [81,132,134,69]). In the present paper, we will focus on contrasting values and trends in the kinetic rate

constants determined from numerical simulation of the breakthrough–elution curves and retained colloid profiles.

4.4. Deposition and re-entrainment rate coefficients

Trends in the deposition and re-entrainment parameters versus ionic strength are shown in Fig. 6. The values of mean k_f , the fraction of irreversible deposition (f_{ir}), and the standard deviation of the deposition rate coefficient distribution in normal space (std. dev. k_f) generally increased with increasing ionic strength for both the 5.7 μm and the 1.1 μm microspheres (Fig. 6). In contrast, the deposition parameters responded variably to fluid velocity (Fig. 7).

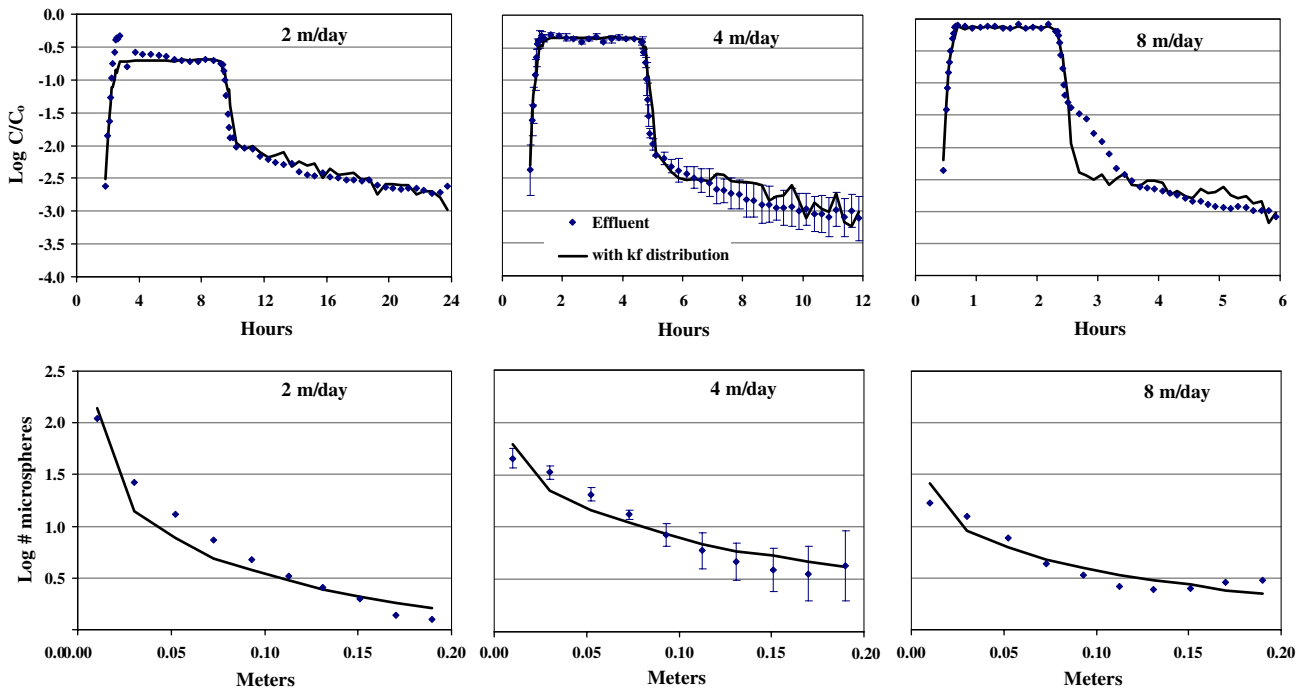


Fig. 4. Flow rate series at ionic strength = 0.006 M, for 1.1- μm microspheres showing effluent breakthrough–elution curves (top), and attached profiles (bottom). Simulations are shown using the particle transport model with an attachment rate (k_f) distribution (solid line). As well, one simulation (dashed line) shows the inability to simultaneously fit both the attached profile and the effluent elution tail.

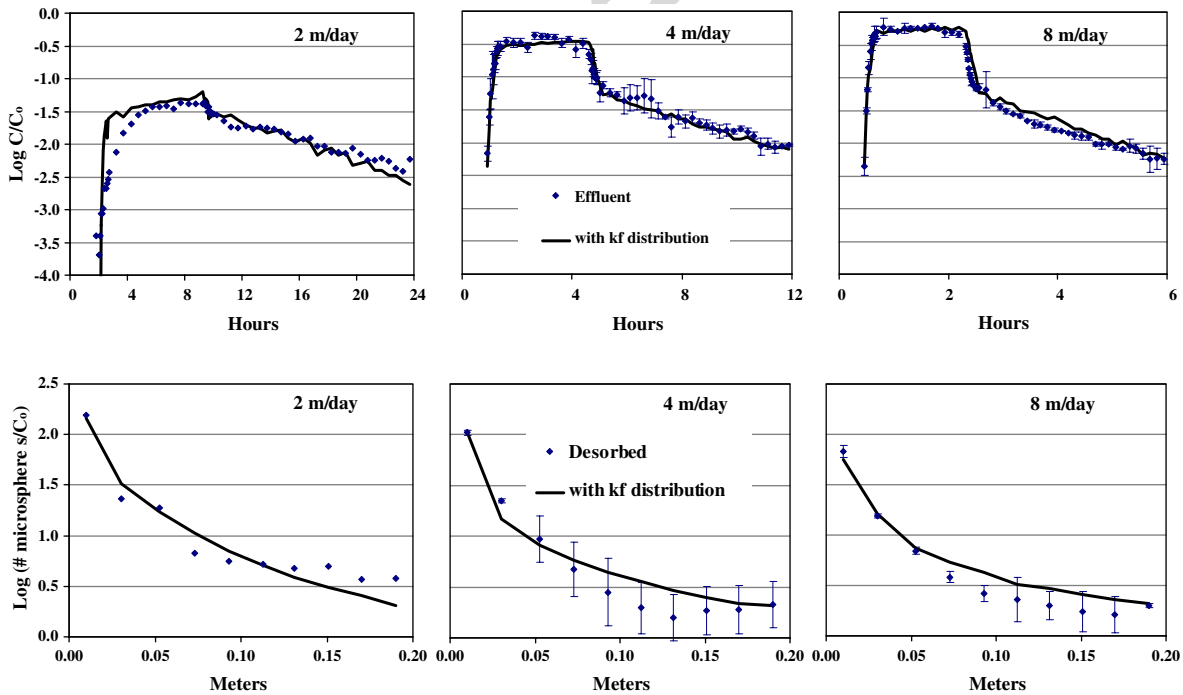


Fig. 5. Flow rate series for 5.7- μm microspheres at ionic strength = 0.006 M, showing effluent breakthrough–elution curves (top), and attached profiles (bottom). Simulations are shown using the particle transport model with an attachment rate (k_f) distribution (solid line).

The re-entrainment parameter, k_r , increased strongly with increases in fluid velocity for both the 5.7 μm and the 1.1 μm microspheres (Fig. 7), whereas this parameter showed no strong relationship with ionic strength (Fig. 6).

4.5. Pull-off forces

Pull-off forces from glass measured using AFM were larger for the 5.7 μm than the 1.1 μm microspheres in qualita-

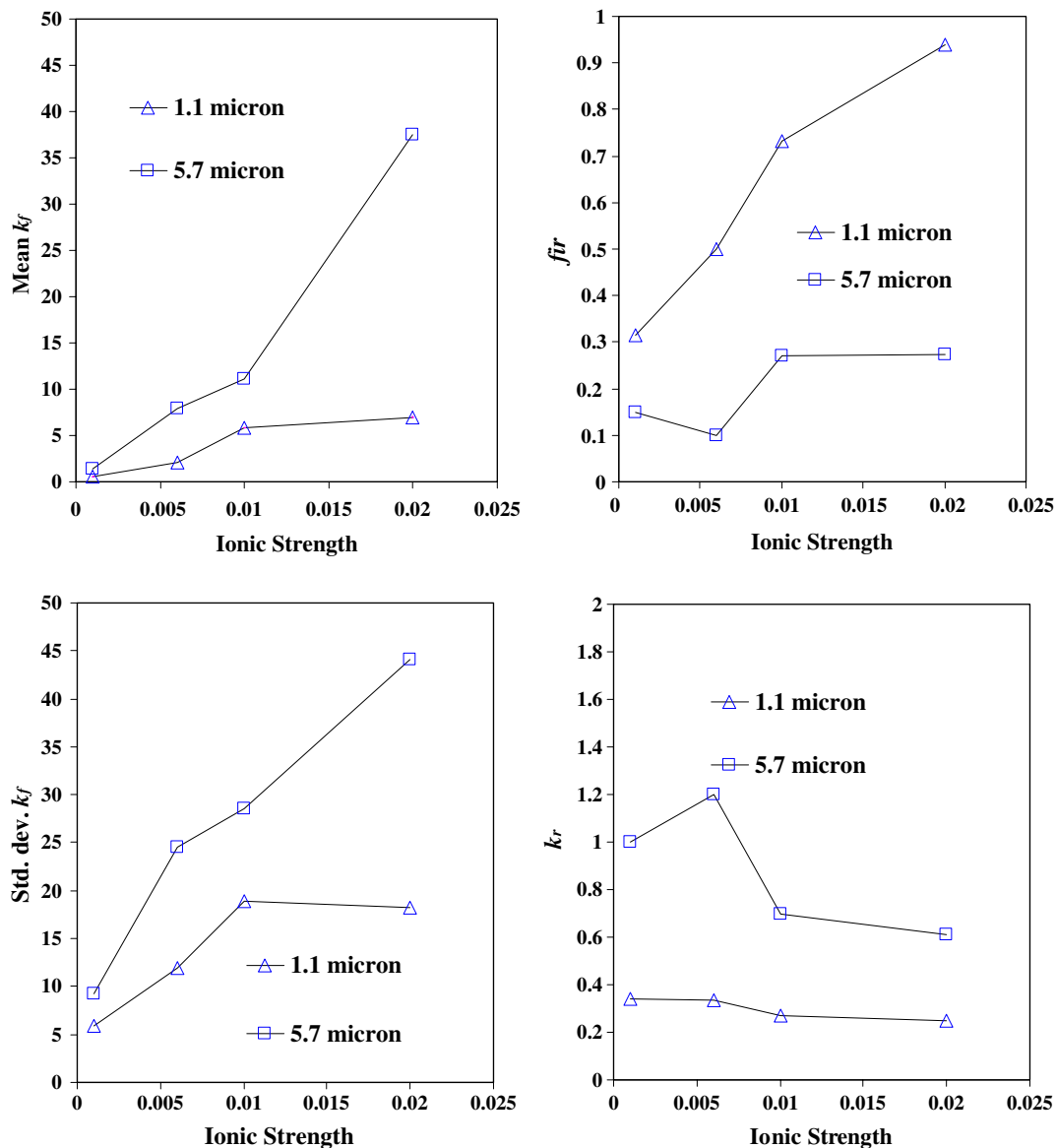


Fig. 6. Kinetic parameters versus ionic strength at 4 m day^{-1} fluid velocity. The kinetic parameters correspond to the simulations shown in Figs. 2 and 3, and are comprised by the mean of the distribution of the deposition rate coefficient in normal space (mean k_f), the standard deviation of the deposition rate coefficient in normal space (std. dev. k_f), the fraction of irreversible deposition (f_{ir}), and the re-entrainment rate coefficient (k_r).

tive agreement with expectations from theory. In contrast to expectations from theory, the pull-off forces for both microspheres showed no clear trend with ionic strength (Table 2), indicating that forces other than electric double layer repulsion and van der Waals attraction (e.g. hydration forces) influenced the measured adhesion forces (Assemi et al., 2005).

5. Discussion

5.1. The contribution of straining

That physical straining significantly contributes to colloid deposition has been argued based on observed retained colloid profiles in which deposition occurs dominantly in

the inlet segment of the porous media column [17,16,15]. That straining is expected to dominantly occur near the inlet is expected on the basis that this physical entrapment occurs in dead-end pores, whereas mobile colloids in continuous flow paths will proceed farther along the column [17]. This behavior is demonstrated in the retained colloid profiles for the $5.7 \mu\text{m}$ microspheres at various ionic strengths (Fig. 3), which show hyper-exponential decreases that are increasingly dominated by deposition in the inlet segment as the ionic strength is decreased. At the two lowest ionic strengths, the shape of the retained profile of the $5.7 \mu\text{m}$ microspheres could not be simulated using a log-normal distribution in colloid deposition rate coefficients. In contrast, the retained colloid profiles for the $1.1 \mu\text{m}$ microspheres (Fig. 2) were not dominated by the inlet

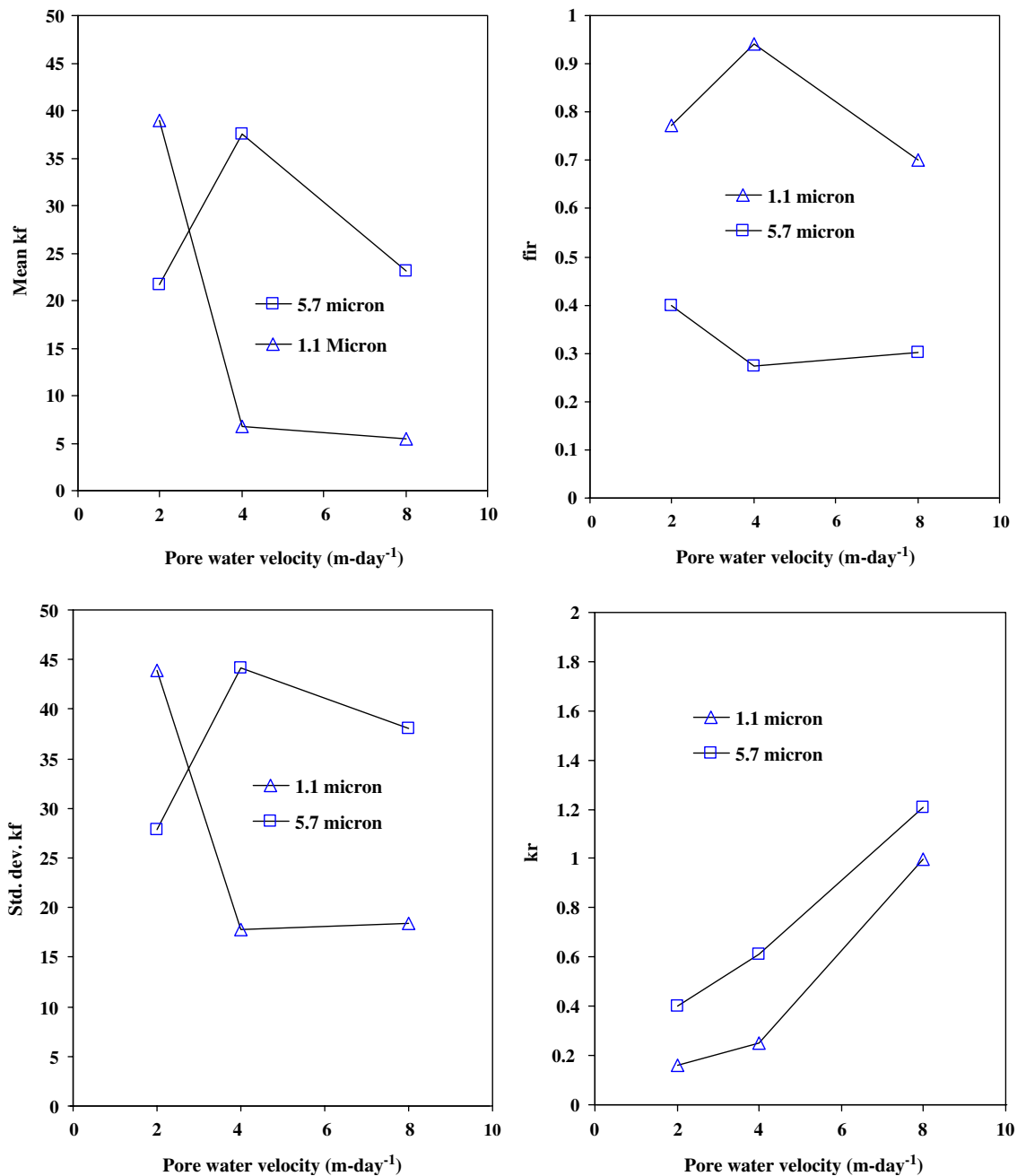


Fig. 7. Kinetic parameters versus fluid velocity at 0.02 M ionic strength. The kinetic parameters correspond to the simulations shown in Figs. 4 and 5, and are comprised by the mean of the distribution of the deposition rate coefficient in normal space (mean k_f), the standard deviation of the deposition rate coefficient in normal space (std. dev. k_f), the fraction of irreversible deposition (f_{ir}), and the re-entrainment rate coefficient (k_r).

segment, even at the lowest ionic strength. The results suggest that straining may be significant for the 5.7 μm microspheres but not the 1.1 μm microspheres under low ionic strength conditions, indicating that the threshold ratio (colloid diameter to mean collector diameter) for straining was between 0.0031 (1.1 $\mu\text{m}/360\mu\text{m}$) and 0.016 (5.7 $\mu\text{m}/360\mu\text{m}$). This threshold range is consistent with the assertion of Bradford et al. [17,16,15], as well as other recent publications [133], that straining occurs at ratios of colloid diameter to mean collector diameter far less than the 0.05 threshold originally suggested by Sakhivadivel [114]. The

ionic strength series shown here demonstrates that while straining may contribute significantly to the observed hyper-exponential retained colloid profiles for the 5.7 μm microspheres, physicochemical deposition dominates at higher ionic strengths.

5.2. Influence of ionic strength on reversibility of deposition

The increase in irreversible deposition (f_{ir}) with increasing ionic strength (Fig. 6) is general among studies that have incorporated this irreversibility parameter (e.g. this

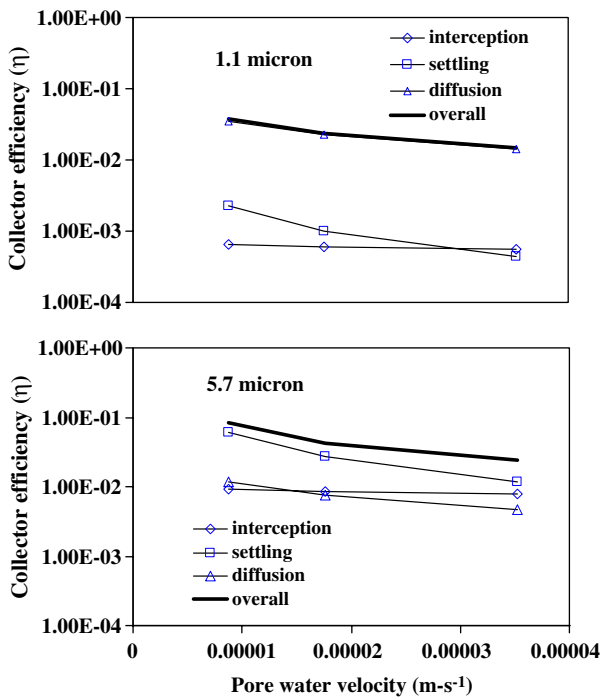


Fig. 8. Calculated collector efficiencies (η) for the 1.1- μm microspheres (top) and 5.7- μm microspheres (bottom). Individual dimensionless contributions from interception only, diffusion, and sedimentation are also shown.

study, Li et al., 2005, [80,129,128]) (Fig. 10). The trend holds for both microspheres and bacteria under the conditions examined. Many of the colloids examined showed significant fractions of reversible deposition at environmentally relevant ionic strengths (e.g. 0.01 M).

The relatively flat trend in f_{ir} versus flow rate observed for both microsphere sizes in Fig. 6 also holds for the microsphere and bacterial transport data in other studies (Li et al., 2005, [80,129,128]) (Fig. 11). Although some of the bacteria flow series do show clear trends in f_{ir} with fluid velocity for a particular colloid and substratum, there is no

Table 2

Pull-off forces for microspheres from AFM (nN) at various ionic strengths

Size (μm)	0.006 M	0.01 M	0.02 M
1.1	0.13 \pm 0.02	0.02 \pm 0.01	0.24 \pm 0.03
5.7	1.52 \pm 0.5	1.31 \pm 0.5	1.38 \pm 0.4

Standard errors are given for 22–30 measurements at three different locations on the glass slide.

agreement between these series on an overall trend among the combined series.

5.3. Influence of hydrodynamic drag on deposition efficiencies

Although the use of distributed deposition rate coefficients improved the simulations of the retained profiles; interpretation of trends in mean k_f and std. dev. k_f was complicated by the fact that these two parameters co-vary (Fig. 7). Interpretation of trends in deposition was therefore simplified by determining overall deposition rate coefficients based on the steady state breakthrough plateau (as traditionally performed). Simulations using overall deposition rate coefficients generated the same trends in k_f and f_{ir} (Table 1) as those generated by simulations using distributions of deposition rate coefficients.

As shown in Table 1, the overall (single) deposition rate coefficient (k_f) was generally larger for the 5.7 μm microspheres relative to the 1.1 μm microspheres across the range of ionic strength and fluid flow conditions, consistent with collector efficiencies calculated from the T–E equation [131,132] (Fig. 8). The process responsible for bringing the microspheres to the grain surfaces under all conditions examined was dominantly diffusion in the case of the 1.1 μm microspheres, whereas settling was the dominant process in the case of the 5.7 μm microspheres (Fig. 8).

The overall deposition rate coefficients (k_f) (Table 1) were converted to deposition efficiencies (α) after determination of the corresponding collector efficiencies using the correlation equation recently developed by Tufenkji

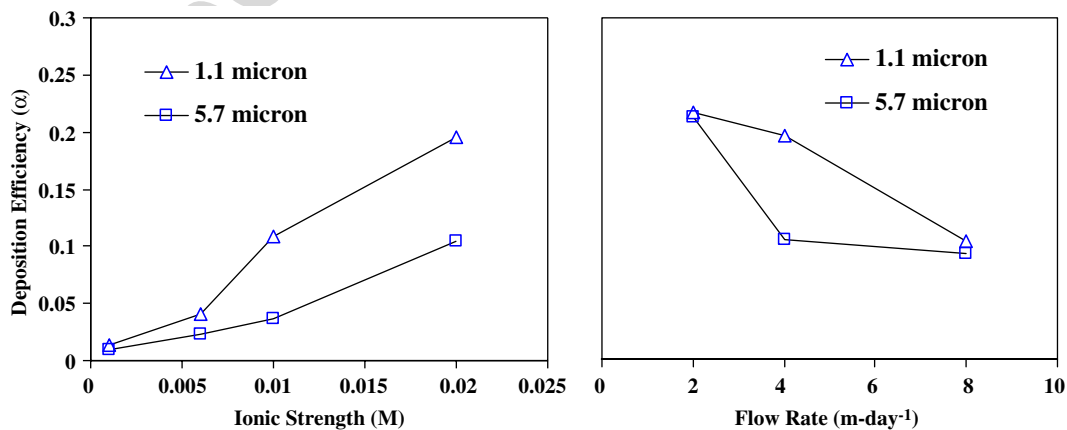


Fig. 9. Deposition efficiencies determined from breakthrough plateaus of the 1.1- μm and 5.7- μm microspheres at different ionic strengths (4 m day⁻¹) (left) and different flow rates (0.02 M) (right).

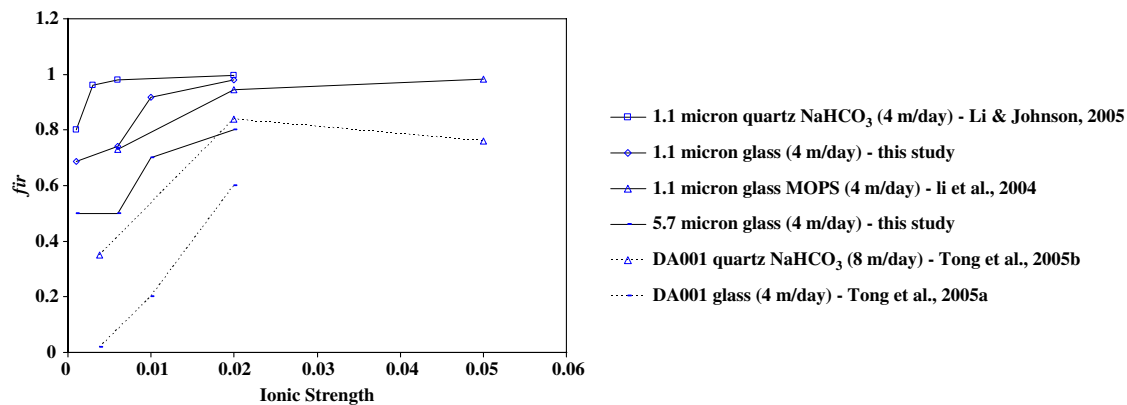


Fig. 10. The fraction of irreversible deposition (f_{ir}) versus ionic strength for biological and non-biological colloids. Data is from the following studies: this study, Li et al. (2005), [80,129,128]. The first number in the series label is the size of the carboxylate-modified latex microsphere, or in the case of biological colloids, the first word denotes the microbe. The second word in all cases is the substratum type. Where the buffer is known, it is defined by the third entry; otherwise the third entry denotes the fluid velocity. The series order in the legend is roughly the same as for the series in the figure. Dashed lines indicate trends for biological colloids. Solid lines correspond to trends for carboxylate polystyrene latex microspheres.

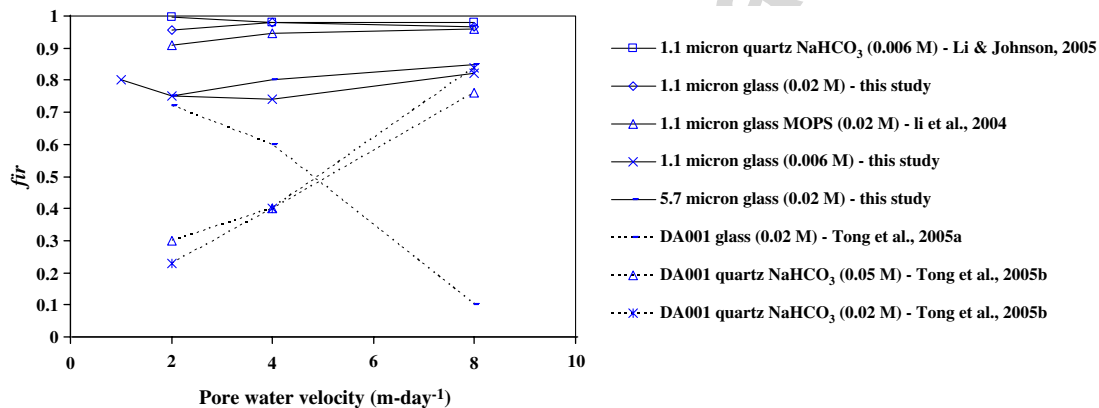


Fig. 11. The fraction of irreversible deposition (f_{ir}) versus fluid velocity for biological and non-biological colloids. Data is from the following studies: this study, Li et al. (2005), [80], Keller et al. (2005), [129,128]. The first number in the series label is the size of the carboxylate-modified latex microsphere, or in the case of biological colloids, the first word denotes the microbe. The second word in all cases is the substratum type. Where the buffer is known, it is defined by the third entry; otherwise the third entry denotes the ionic strength (M). The series order in the legend is roughly the same as for the series in the figure. Dashed lines indicate trends for biological colloids. Solid lines correspond to trends for carboxylate polystyrene latex microspheres.

and Elimelech [131], as described in detail in Li et al. (2005). Fig. 9 (left side) demonstrates that for both microsphere sizes, the value of the deposition efficiencies increased with increasing ionic strength, concomitant with decreasing heights of the energy barriers to deposition, and increasing depths of the energy minima (Fig. 12). Deposition efficiencies for the 5.7 μm microspheres were a factor of two to three less than those of the 1.1 μm microspheres (Fig. 9), in qualitative agreement with larger energy barriers to deposition for the 5.7 μm microspheres relative to the 1.1 μm microspheres at a given ionic strength (Fig. 12). Alternatively, the lower deposition efficiencies may represent the greater hydrodynamic drag experienced by the 5.7 μm microspheres relative to the 1.1 μm microspheres at a given flow rate, as discussed below.

The deposition efficiencies for both the 5.7 and 1.1 μm microspheres decreased with increasing fluid velocity (Fig. 9). Similar trends were observed for the 1.1 μm micro-

spheres under equivalent ionic strength and fluid velocity conditions in an impinging jet system [18] as well as in a similar porous media system (Li et al., 2005). The observed decrease in deposition efficiency with increasing fluid velocity reflects the different trends of the deposition flux versus fluid velocity in the presence versus the absence of an energy barrier. Specifically, the deposition flux in the presence of an energy barrier increases less with increasing fluid velocity, or may even decrease with increasing fluid velocity [78,138,88], relative to the deposition flux in the absence of an energy barrier. These different trends in the presence relative to the absence of an energy barrier suggest vulnerability to hydrodynamic drag in the presence of an energy barrier. Recently, decreased deposition efficiencies with increasing fluid velocity were reported in sand (median grain size 350 μm) for three different colloids (MS2 bacteriophage, 0.05 μm and 3.0 μm carboxylate-modified polystyrene latex microspheres) and fluid velocities ranging

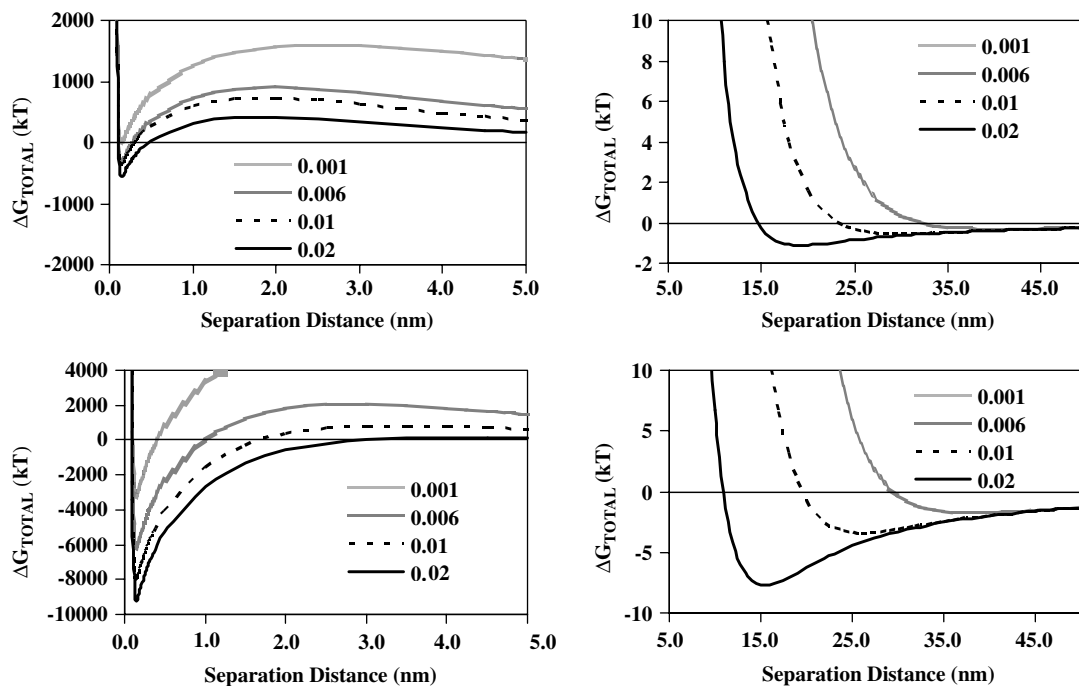


Fig. 12. DLVO interaction energy profiles for the 1.1 mm (top) and 5.7 mm (bottom) microspheres, within 5 nm (left), and between 5 and 50 nm (right), from the surface. Note that repulsive energies greater than 10 kT are maintained at separation distances greater than 50 nm at the 0.001 M ionic strength condition.

1.4–14 m day⁻¹ [76]. However, the authors did not elaborate on the possible significance of this trend since the focus of the article was on differential advection. Decreased microsphere deposition efficiency with increasing fluid velocity was observed on a micropatterned surface (positively and negatively charged stripes) in a radial stagnation point flow system [42] suggesting that “interplay of electric double layer and hydrodynamic forces” mitigated deposition.

Fig. 13 shows trends in deposition efficiency (α) versus fluid velocity in porous media from various studies (this study, Li et al., 2005, [80], Keller et al., 2005, [129,128]). Colloid sizes among these studies ranged from 0.025 μm bacteriophage MS2 to 1.1 mm microspheres and bacteria to 5.7 μm microspheres. The porous media used in these studies were either glass beads, quartz, or natural sand, with median grain diameters of 360 μm (this study), 510 μm (Li et al., 2005, [80,129,128]), and 350 μm [76], respectively. The differences in the magnitudes of the deposition efficiencies are likely related to the magnitudes of the energy barriers to deposition among the different studies. The overall trend yields about factor of four decreases in deposition efficiency correspondent with factor of 10 increases in fluid velocity for the conditions examined. The overall trend of decreasing deposition efficiency with increasing fluid velocity is not as clear for the bacteria (DA001) in some experiments (i.e. [128]). The trends for biological colloids are shown as dashed lines in Fig. 13. That bacteria follow less closely the overall trend may be due to the structural softness of bacterial cells relative to microspheres and bacteriophage, allowing deformation in

response to hydrodynamic drag. The overall trend of decreasing deposition efficiency with increasing flow rate for biological and non-biological demonstrates a mitigating effect of hydrodynamic drag on the deposition of colloids in the presence of an energy barrier.

Simulations of colloid transport in simple shear systems demonstrate that deposition flux to the primary energy minimum decreases with increasing flow rate under conditions where the energy barrier to deposition is small relative to the secondary energy minimum. Deposition flux is reduced due to lateral translation of secondary minimum-associated colloids in response to tangential hydrodynamic drag [104,150]. In our system, the formidable energy barriers to deposition (Fig. 12) would seem to preclude this indirect effect of hydrodynamic drag as a cause of decreased deposition efficiency with increasing fluid velocity. It therefore seems prudent to consider other possibilities; e.g., that the observed decrease in deposition efficiency with increasing fluid velocity represents re-entrainment of microspheres during incipient deposition, or that it represents other effects of hydrodynamic drag.

5.4. Influence of hydrodynamic drag on re-entrainment rate

For both colloid sizes, the re-entrainment rate (k_r) increased with increasing flow rate (Fig. 9), demonstrating that re-entrainment under non-perturbed conditions was influenced by hydrodynamic drag. The few studies that have previously examined bacterial detachment under non-perturbed conditions in porous media concluded that the re-entrainment rate coefficient (k_r) was independent of

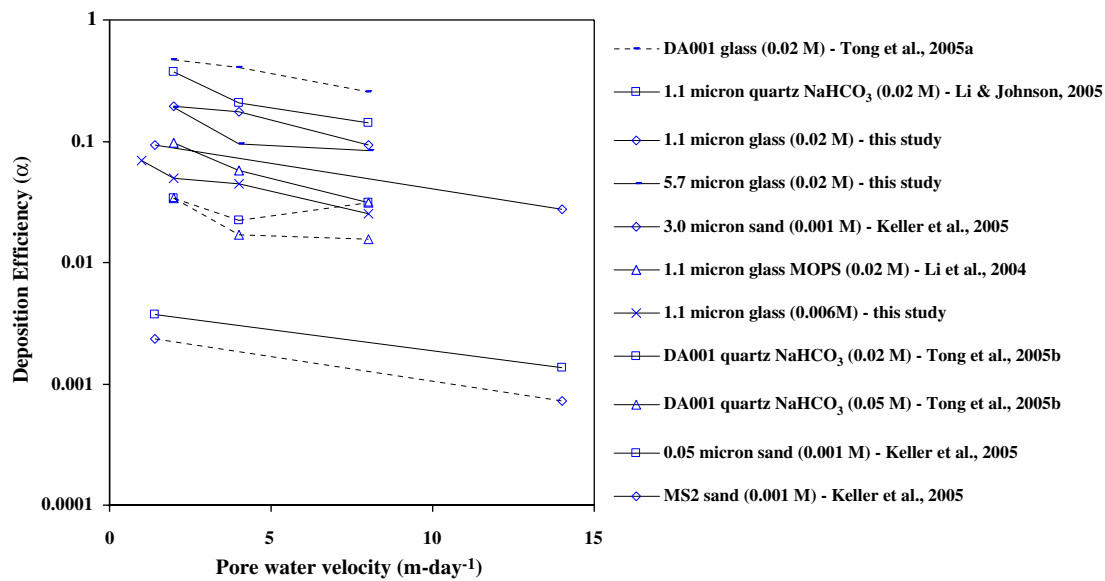


Fig. 13. Deposition efficiencies (α) versus flow rate ionic strength for biological and non-biological colloids. Data is from the following studies: this study, Li et al. (2005), [80], Keller et al. (2005), [129,128]. The first number in the series label is the size of the carboxylate-modified latex microsphere, or in the case of biological colloids, the first word denotes the microbe. The second word in all cases is the substratum type. Where the buffer is known, it is defined by the third entry; otherwise the third entry denotes ionic strength. The series order in the legend is roughly the same as that from top to bottom in the figure. Dashed lines indicate trends for biological colloids. Solid lines correspond to trends for carboxylate polystyrene latex microspheres.

pore water velocity under the conditions of the experiments [125,59]. More recently, studies examining the transport of Ca-saturated smectite clay colloids in quartz sand under varied ionic strength and flow conditions [26] showed that the re-entrainment rate increased with increasing flow rate, and decreased with increased ionic strength. However, the analysis did not extend beyond these useful observations.

Studies performed in simple shear systems have been more definitive with respect to the mechanism of detachment under non-perturbed conditions. For example, Meinders and Busscher [86] used a parallel plate flow chamber and video microscope to directly observe polystyrene microsphere detachment rates from glass. The detachment rates ranged from $1\text{E}-6$ to $5\text{E}-3 \text{ s}^{-1}$ for a shear rate range of 15 to 200 s^{-1} , respectively, in the presence of mobile colloids; and $4\text{E}-7$ to $1.2\text{E}-6 \text{ s}^{-1}$ for the same shear rate range in the absence of mobile colloids. Although the detachment rate increased with increased shear, the authors focused on the observation that detachment rates increased with increasing concentration of mobile colloids. The latter observation was the basis for concluding that hydrodynamic collision was an important contributor to detachment kinetics in the presence of mobile particles.

The generality of increasing re-entrainment rate coefficient with increasing fluid velocity is demonstrated in Fig. 14, which combines results from experiments examining the transport of biological and non-biological colloids (this study, Li et al., 2005, [80], Keller et al., 2005, [129,128]). All of the series save one show increasing k_r with increasing fluid velocity. The one series that breaks from the trend (DA001 in quartz at 0.02 M) is the sole series that was not supported by replicate experiments [128]. The data

from a spectrum of studies demonstrates convincingly that under non-perturbed conditions in the presence of an energy barrier to deposition, hydrodynamic drag drives re-entrainment of biological and non-biological colloids.

The relatively flat trend in k_r versus ionic strength observed for the 1.1 μm microspheres. Fig. 6 also holds for the microsphere and bacterial transport data in the other studies (Li et al., 2005, [80,129,128]) (Fig. 15). The overall data set may suggest even a slight decrease in k_r with increasing ionic strength, consistent with increased f_{ir} with increasing ionic strength.

5.5. Environment of deposition: Primary energy minimum

Under a given ionic strength and flow condition, the 5.7 μm microspheres consistently showed lesser f_{ir} and greater k_r relative to the 1.1 μm microspheres. This demonstrates that the large microspheres were deposited more reversibly than the smaller microspheres. The greater reversibility of deposition of the 5.7 μm microspheres may relate to the environment of deposition, e.g. the primary or secondary minimum.

Deposition of the 1.1 μm microspheres was significant in corresponding impinging jet cell experiments, which were conducted under the same ionic strength and surface velocity conditions examined here [18]. In contrast to porous media, an impinging jet system restricts observed deposition to that “within” the primary energy minimum, since the flat surface contains no zones of flow stagnation in which to retain secondary minimum-associated colloids.

The maximum hydrodynamic torque estimated for the 1.1 μm microspheres in the impinging jet was $9.16\text{E}-20$

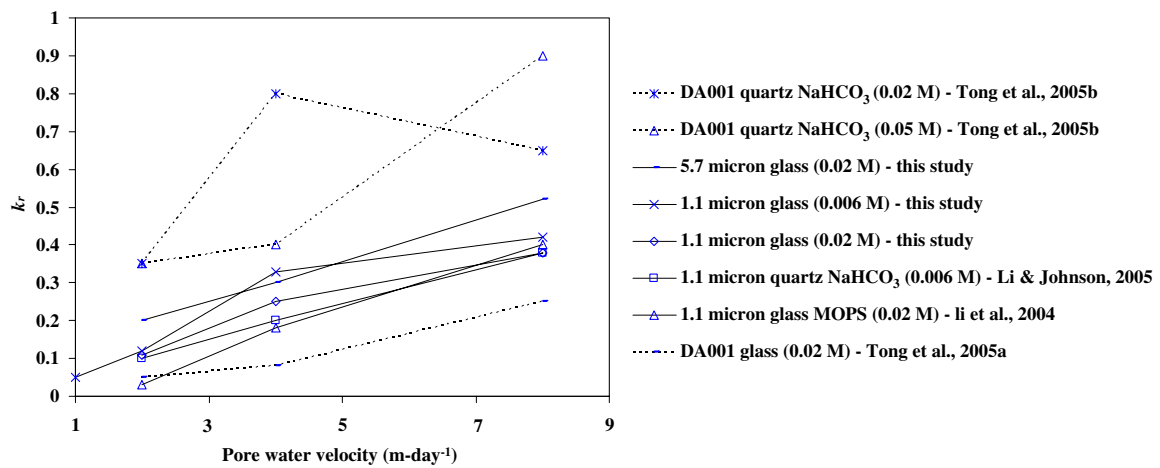


Fig. 14. Re-entrainment rates (k_r) versus flow rate for biological and non-biological colloids. Data is from the following studies: this study, Li et al. (2005), [80,129,128]. The first number in the series label is the size of the carboxylate-modified latex microsphere, or in the case of biological colloids, the first word denotes the microbe. The second word in all cases is the substratum type. Where the buffer is known, it is defined by the third entry; otherwise the third entry denotes ionic strength. The series order in the legend is roughly the same as that from top to bottom in the figure. Dashed lines indicate trends for biological colloids. Solid lines correspond to trends for carboxylate polystyrene latex microspheres.

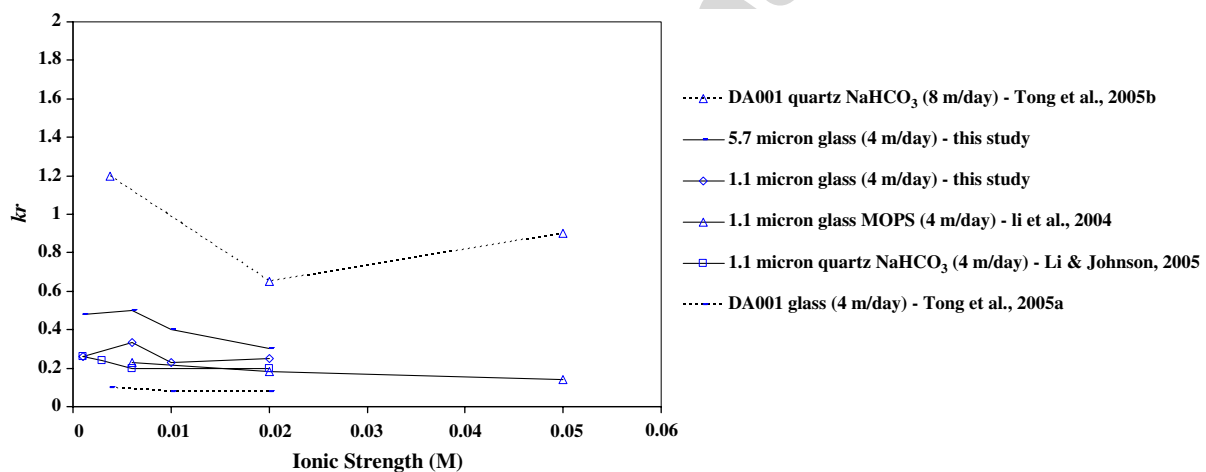


Fig. 15. Re-entrainment rates (k_r) versus ionic strength for biological and non-biological colloids. Data is from the following studies: this study, Li et al. (2005), [80,129,128]. The first number in the series label is the size of the carboxylate-modified latex microsphere, or in the case of biological colloids, the first word denotes the microbe. The second word in all cases is the substratum type. Where the buffer is known, it is defined by the third entry; otherwise the third entry denotes fluid velocity. The series order in the legend is roughly the same as that from top to bottom in the figure. Dashed lines indicate trends for biological colloids. Solid lines correspond to trends for carboxylate polystyrene latex microspheres.

N m (Table 3) [18], whereas the maximum adhesive torque for the 1.1 μm microspheres estimated based on AFM “pull-off” forces was $1.2\text{E}-18$ N m (at 4 m day^{-1}), a value that is far higher than the maximum hydrodynamic torque,

and which thereby supports the observed deposition of the 1.1 μm microspheres in the impinging jet system.

Notably, under equivalent conditions to those described above, the 5.7- μm microspheres were not deposited in the

Table 3
Range of measured AFM pull-off forces with corresponding contact areas and adhesive torques calculated according to Eqs. (7) and (8)

Size (μm)	AFM pull-off forces (nN) highest/lowest	Contact radius (nm)	Adhesive torque (N m) highest/lowest	Hydrodynamic torque (N m) highest/lowest 4 m day^{-1}	Fluid velocity at one radius (m s^{-1}) highest/lowest
1.1	$0.24 \pm 0.03/0.020 \pm 0.01$	5.1/2.2	$1.2\text{E}-18/4.4\text{E}-20$	$9.2\text{E}-20/9.4\text{E}-21$	$6.8\text{E}-06/6.9\text{E}-07$
5.7	$1.5 \pm 0.50/1.3 \pm 0.50$	16.3/15.5	$2.5\text{E}-17/2.0\text{E}-17$	$1.2\text{E}-17/1.3\text{E}-18$	$3.4\text{E}-05/3.5\text{E}-06$

Range of calculated surface fluid velocities at one colloid radius from the surface for the 4 m day^{-1} average pore fluid velocity condition, calculated according to Eqs. (5) and (6). Hydrodynamic torques associated with surface velocities according to Eq. (4). The surface fluid velocities and hydrodynamic torques for the 2 m day^{-1} and 8 m day^{-1} are factors of 2 below and above, respectively, the values for the 4 m day^{-1} condition.

impinging jet cell [18]. The maximum hydrodynamic torque estimated for the 5.7 μm microspheres in the impinging jet was $1.23\text{E}-17$ N m (at 4 m day^{-1} flow rate) (Table 3), whereas the maximum adhesive torque for the 5.7 μm microspheres estimated based on AFM “pull-off” forces was $2.5\text{E}-17$ N m. The lack of deposition of 5.7 μm microspheres in the impinging jet is consistent with the near parity of the maximum adhesive and hydrodynamic torques. The lack of deposition of the 5.7 μm microspheres in the impinging jet system indicates that deposition of these microspheres in the glass bead packed column occurred by other mechanisms, e.g. by straining or within flow stagnation zones in the porous media.

The greater reversibility of deposition of the 5.7- μm microspheres relative to the 1.1- μm microspheres in the glass beads is also supported by the torque ratios. For example, for the 4 m day^{-1} flow condition, the ratio of the highest adhesive torque to the highest hydrodynamic torque was >17 for the 1.1 μm microspheres, and was <2 for the 5.7 μm microspheres (Table 3). The hydrodynamic torques for the 2 m day^{-1} and 8 m day^{-1} conditions are a factor of 2 below and above, respectively, those for the 4 m day^{-1} condition. That the lowest adhesive torque is estimated to be within about a factor of two of the highest hydrodynamic torque for the 5.7- μm microspheres supports the possibility that the steady elution of low concentrations of microspheres (especially the 5.7 μm microspheres) represents re-entrainment from the primary energy minimum. Furthermore, the estimated adhesive torques may represent averages within a distribution [75,6,148,49,50], as demonstrated by the solution chemistry perturbation-driven release of natural mineral colloids from sediment, which yielded eluted colloid concentrations that decayed according to a power law [49], indicating heterogeneity in the attached particle population that likely originated from the different local environments surrounding each particle. A distribution in adhesive torques may also be expected on the basis that a distribution in deposition rate coefficients is required to simulate the retained microsphere profiles (e.g. [81]).

The microsphere–glass bead contact radii estimated using Eq. (8) ranged from 6.8 to 16.3 nm. If the glass bead surface were perfectly smooth (lacking surface asperities), these contact radii would serve as the lever arms defining the adhesive torque, assuming that rolling is initiated by “tipping” the microsphere off the contact radius [112]. Because rolling is likely initiated by microsphere deformation in the contact area, rather than tipping, the lever arm defining the adhesive torque may be smaller than those estimated using Eq. (8). However, since the glass bead surfaces are not perfectly smooth, protrusions may also enhance or decrease the effective lever arm. If the protrusions are spaced such that microspheres rest against them, they will enhance the effective lever arm [34]. Simple trigonometry indicates that even a 0.5 nm high protrusion can provide an effective lever arm of 23.5 nm for a 1.1 μm colloid, a value that is greater than corresponding the lever arms esti-

mated from Eq. (8) (Table 3). Alternatively, if the microspheres rested atop closely spaced surface asperities, the actual contact areas may be decreased relative to those expected from Eq. (8) (e.g., Eichenlaub et al., 2004). Measured root-mean-square surface roughness of glass beads was measured to be 15.0 ± 1.9 nm, with distances between asperities being much greater than the size of the 1.1 μm microspheres [119], indicating that the retained microspheres may rest against asperities. The estimated contact radii (Table 3) may either over-estimate the effective lever arm (due to microsphere deformation at contact area), or under-estimate the effective lever arm (due to asperities). In the absence of easily implemented expressions to account for surface roughness, we speculate that the estimated contact radii, and the corresponding adhesive torques (Table 3), represent a compromise between considerations that were beyond our ability to quantify. The torque balance does not disprove the possibility of detachment from the primary energy minimum.

5.6. Environment of deposition: secondary energy minimum

The experimental results can also be interpreted to indicate reversible deposition of the microspheres “within” the secondary energy minimum. The most direct evidence for colloid deposition in secondary minima comes from experiments involving perturbation of solution chemistry. O’Melia and co-workers [52,51] demonstrate reversibility of deposition of the majority of colloids upon reduction of solution ionic strength, which should not occur if the colloids were deposited in the primary energy minimum, since the barrier to detachment from the primary energy minimum is increased as ionic strength is decreased (Fig. 12). Unpublished results from our laboratory also demonstrate elution of at least half of the deposited population upon introduction of low ionic strength water. In contrast, introduction of low ionic strength solution to the impinging jet cell yielded insignificant re-entrainment of deposited microspheres, consistent with their expected deposition “within” primary energy minima, as described below.

Colloids associated with secondary energy minima would be expected to translate across the porous media grain surfaces due to hydrodynamic drag tangential to the surfaces. Secondary minimum-associated colloids would potentially be retained in porous media in zones of flow stagnation (e.g. rear stagnation points or leeward sides of protrusions). In contrast to porous media, colloid deposition within an impinging jet system is restricted to “within” the primary energy minimum, since the smooth flat surface does not contain zones of flow stagnation within which to retain secondary minimum-associated colloids. Under conditions of secondary minimum deposition, and equivalent solution chemistry and surface fluid velocity conditions, one would expect greater deposition in a porous media relative to an impinging jet due to the expected presence of zones of flow stagnation in the porous media.

Enhanced deposition efficiencies in porous media relative to impinging jet systems were observed by Brow et al. [18] for the 1.1 μm microspheres in quartz substrata under the same solution ionic strength and surface velocity conditions examined here. Experiments comparing deposition efficiencies in porous media relative to impinging jet systems also show enhanced deposition of bacteria in porous media [107,147]. These results indicate that the presence of zones of flow stagnation enhances colloid deposition.

5.7. Dual deposition

The above and related work demonstrates that colloid deposition in porous media in the presence of an energy barrier likely involves deposition “within” both primary energy minima and the secondary energy minima, with the balance among them being determined by characteristics such as surface and solution chemistries, colloid sizes, and fluid velocity. Dual deposition modes of carboxylate-modified microspheres were previously demonstrated in glass beads [132,134,135], where a large fraction of the deposited colloids were eluted upon introduction of low ionic strength water (i.e. deposited in secondary minimum). However, an additional smaller fraction was eluted upon introduction of high pH solution intended to reverse the charge on localized patches of attractive surface charge (i.e. deposited in primary minimum).

Although dual deposition modes are expected to govern colloid transport in porous media, the relationship of this dual deposition behavior to the observed deviations from filtration theory is not yet clear. Dual deposition may be driven at least in part by heterogeneity in surface characteristics among the colloid population, as proposed more than a decade ago [3]. A very wide (e.g. log-normal) distribution in deposition rate coefficients may result from very mild distributions in surface characteristics [81]. Surface charge heterogeneity is observed even on single microspheres [43,124] and heterogeneity of surface characteristics has been demonstrated for bacterial cells [72], suggesting the possibility that the collision efficiency of an individual colloid may depend on its orientation upon collision with the collector, thus effectively producing heterogeneity among an apparently homogenous colloid population.

Tufenkji and Elimelech [135] suggest that distributed surface characteristics on both the particle and the porous media are pre-requisite to a wide distribution of deposition rates. Although we disagree with this notion as a requirement for wide distributions [81], we can certainly expect that porous media heterogeneity influences deposition rate coefficients. The dual deposition model of Tufenkji and Elimelech [135] utilized a bimodal sum of two Gaussian distributions to represent the overall distribution of deposition rate coefficients [132], implying that one of the Gaussian distributions represents particles, and the other Gaussian distribution represents the porous media. However, a simple sum of distributions would not reflect the actual interaction between two distributed properties.

Additionally, the bimodal distribution cannot represent heterogeneity on the porous media, since the high values in the distribution by definition result in rapid deposition, i.e. deposition at the inlet end of the column, which is inconsistent with a re-packed column where the full range of deposition rate coefficients would occur anywhere along the length of the re-packed column, not only the inlet [69]. In short, given presently articulated mechanisms, heterogeneity that is evenly distributed across a re-packed porous media can *widen* the distribution of deposition rate coefficients, but it cannot *generate* such a distribution.

5.8. Sustaining mechanisms of re-entrainment

An important characteristic of re-entrainment in the absence of perturbations is that it extends over long periods of time and appears to be self-sustaining. Likewise, the brief pulse of large concentrations of re-entrained colloids that results from perturbations in solution chemistry or flow are followed by sustained low concentrations of colloids (extended tailing) [52,51,49]. The sustained re-entrainment that occurs in the absence of perturbations can potentially arise from a number of processes acting on primary minimum-attached colloids: e.g. hydrodynamic collision between mobile and attached colloids, and microscale fluctuations in the hydrodynamic field at the grain surface. That hydrodynamic collision between mobile and attached colloids enhances detachment of attached particles has been established based on force balance calculations [32,31], and experimental studies in simple shear systems [87,88]. These studies indicate that hydrodynamic interaction between deposited and mobile colloids in simple shear systems causes the normal force acting on the deposited particles to fluctuate even for relatively large particle separations, resulting in the escape of weakly bound colloids. The deformability of bacteria would be expected to decrease the energy of hydrodynamic collision relative to other colloids. However, after observing increased detachment of bacteria in the presence versus the absence of mobile bacteria, Meinders et al. [89] concluded that hydrodynamic collision was relevant to bacterial re-entrainment. Although hydrodynamic collision was suggested in field experiments involving adhesion deficient soil bacteria, it was not conclusively demonstrated [65,67]. Hydrodynamic collision would dictate that colloid re-entrainment rates should vary between the injection and elution stages of colloid transport experiments. In contrast, presently published colloid transport models for porous media tend to relate the overall rate of re-entrainment to the retained colloid concentration only. Significant hydrodynamic collision should manifest as a dependence of the deposition rate coefficient on the influent concentration (e.g. [14]).

Microscale fluctuations in the hydrodynamic field at the grain surface may also potentially result from re-entrainment. The grain surface excluded from subsequent colloid deposition due to the presence of an attached colloid (excluded area) is directly related to the repulsive energy

between the colloids, as well as the extent to which the attached colloid impinges on the hydrodynamic field. The excluded area extends asymmetrically leeward of the attached colloid as the fluid velocity increases, as observed directly in simple shear systems [86,87,108,30,2], and as inferred in porous media experiments [77]. We speculate that the presence of this hydrodynamic “shadow” contributes to a dynamic character of the hydrodynamic field at the grain surface that may sustain re-entrainment. For example, detachment of a given colloid would result in greater hydrodynamic drag experienced by attached colloids residing within what was the hydrodynamic shadow of a newly detached particle. Although initial colloid deposition would not be expected to occur within a hydrodynamic shadow, colloid translation following initial deposition may concentrate colloids on the leeward sides of grain surface asperities and attached colloids.

Deposition in the secondary minimum provides opportunities for sustained re-entrainment via hydrodynamic drag, including: (1) decreased colloid retention capacity due to reduction of stagnation flow zone volumes; (2) increased diffusion “out” of secondary minima (e.g. [52]) driven by increased colloid concentration gradients away from zones of accumulation (e.g. rear stagnation points); (3) increased magnitude of hydrodynamic collisions between mobile and surface-associated colloids; (4) increased dominance of hydrodynamic drag torques relative to adhesive torques created by protrusions.

5.9. Boundary conditions and hydrodynamic drag

The determination that primary minimum-associated and secondary minimum-associated colloids are vulnerable to hydrodynamic drag presents a much greater opportunity for re-entrainment of colloidal populations, and dynamic deposition and re-entrainment relative to traditional expectations. Deposited colloids in porous media may under some circumstances be held much more reversibly (and dynamically) than has been traditionally assumed, as suggested by Johnson et al. [68], and recently inferred by Kim and Tobiason (2004), and as recently demonstrated by Tong et al. [129].

The above findings call for the development of models that will take into account the influence of tangential hydrodynamic drag on deposition “within”, and re-entrainment “from”, the primary and secondary energy minima. Existing models assume that deposition occurs “within” the primary minimum, which is treated as a perfect sink boundary where the colloid is effectively removed from solution and is no longer subject to hydrodynamic drag [40,150]. These models are accurate when an energy barrier is absent, but predict zero colloid attachment in the presence of a significant energy barrier. In some models accounting for a small energy barrier (e.g. a few kT) and a large secondary energy minimum (e.g. more than a few kT), deposition “within” the primary minimum is moderated by the presence of a secondary energy minimum,

“within” which colloids are relatively concentrated. Lateral translation of the secondary minimum-associated colloids by tangential hydrodynamic drag reduces the flux of colloids across the energy barrier to the primary minimum (Prieve and Lin, 1999) [150].

Improved model boundary conditions are needed to describe the direct influence of tangential hydrodynamic drag on colloid deposition and re-entrainment. These boundary conditions will need to incorporate the balance of adhesive and hydrodynamic forces relevant to the primary and secondary energy minima. They will need to consider the hydrodynamic flow field, e.g. the volume of zones of flow stagnation relative to the overall pore domain, which will be governed by grain morphology and fluid velocity. Development of these models will necessarily require direct observation at the pore scale to guide up-scaling to the continuum scale.

Acknowledgements

The authors greatly appreciate the expert efforts of Dr. Mitchell Small, Associate Editor of Environmental Science & Technology, and his assistant Mrs. Karen Peretin, in execution of thorough and efficient reviews of our recent manuscripts that formed the basis for this paper. This material is based upon work supported by the National Science Foundation under Grant No. 0087522. Any opinions, findings, and conclusions or recommendations expressed in this material are those of the authors and do not necessarily reflect the views of the National Science Foundation.

References

- [1] Abu-Lail NI, Camesano TA. Role of lipopolysaccharides in the adhesion, retention, and transport of *Escherichia coli* JM109. *Environ Sci Technol* 2003;37(10):2173–83.
- [2] Adamczyk Z, Siwek B, Szyk L. Flow induced blocking effects in adsorption of colloid particles. *J Colloid Interface Sci* 1995;174:130–41.
- [3] Albinger O, Biesemeyer BK, Arnold RG, Logan BE. *FEMS Microbiol Lett* 1994;124:321–6.
- [4] Bales RC, Gerba CP, Grondin GH, Jensen SL. Bacteriophage transport in sandy soil and fractured tuff. *Appl Environ Microb* 1989;55(8):2061–7.
- [5] Bales RC, Li SM, Yeh TCJ, Lenczewski ME, Gerba CP. *Water Resour Res* 1997;33:639–48.
- [6] Barouch E, Wright TH, Matejević E. Kinetics of particle detachment. *J Colloid Interface Sci* 1987;118(2):473–81.
- [7] Baygents JC, Glynn Jr JR, Albinger O, Biesemeyer BK, Ogden KL, Arnold RG. *Environ Sci Technol* 1998;32:1596–603.
- [8] Bergendahl J, Grasso D. Prediction of colloid detachment in a model porous media: hydrodynamics. *Chem Eng Sci* 2000;55:1523–32.
- [9] Bergendahl J, Grasso D. Prediction of colloidal detachment in a model porous media: thermodynamics. *AIChE J* 1999;45(3):475–84.
- [10] Bergendahl J, Grasso D. Mechanistic basis for particle detachment from granular media. *Environ Sci Technol* 2003;37(10):2317–22.
- [11] Bhattacharjee S, Ko CH, Elimelech M. DLVO interaction between rough surfaces. *Langmuir* 1998;14:3365–75.
- [12] Bolster CH, Mills AL, Hornberger G, Herman J. *Water Resour Res* 1999;35:1797–808.

- [13] Bolster CH, Mills AL, Hornberger G, Herman J. *Ground Water* 2000;38:370–5.
- [14] Bradford SA, Bettahar M. Concentration dependent colloid transport in saturated porous media. Presentation at 229th ACS national meeting session “colloid separation and transport in aquatic environments”, San Diego, CA, March 13–17, 2005.
- [15] Bradford SA, Bettahar M, Simunek J, van Genuchten MT. Straining and attachment of colloids in physically heterogeneous porous media. *Vadose Zone J* 2004;3:384–94.
- [16] Bradford SA, Simunek J, Bettahar M, Van Genuchten MT, Yates SR. *Environ Sci Technol* 2003;37:2242–50.
- [17] Bradford SA, Yates SR, Bettahar M, Simunek J. Physical factors affecting the transport and fate of colloids in saturated porous media. *Water Resour Res* 2002;38(12):1327–38.
- [18] Brow CN, Li X, Rička J, Johnson WP. Comparison of microsphere deposition in porous media versus simple shear systems. *Colloids Surf A: Physicochem Eng Aspects* 2005;253(1–3):125–36.
- [19] Brown DG, Stencel JR, Jaffé PR. Effects of porous media preparation on bacteria transport through laboratory columns. *Water Res* 2002;36:105–14.
- [20] Buddemier RW, Hunt JR. Transport of colloidal contaminants in groundwater: radionuclide migration at the Nevada test site. *Appl Geochem* 1988;3(5):535–48.
- [21] Burks GA, Velegol SB, Paramonova E, Lindenmuth BE, Feick JD, Logan BE. Macroscopic and nanoscale measurements of the adhesion of bacteria with varying outer layer surface composition. *Langmuir* 2003;19:2366–71.
- [22] Camesano TA, Logan BE. Probing bacterial electrosteric interactions using atomic force microscopy. *Environ Sci Technol* 2000;34:3354–62.
- [23] Camesano TA, Logan BE. Influence of fluid velocity and cell concentration on the transport of motile and nonmotile bacteria in porous media. *Environ Sci Technol* 1998;32:1699–708.
- [24] Champ DR, Shroeter J. Bacterial transport in fractured rock – a field scale tracer test at the Chalk river nuclear laboratories. *Water Sci Technol* 1988;20(11–12):81–7.
- [25] Cleveland JP, Manne S, Bocek D. A nondestructive method for determining the spring constant of cantilevers for scanning force microscopy. *Rev Sci Instrum* 1993;64(2):403–5.
- [26] Compère F, Porel G, Delay F. Transport and retention of clay particles in saturated porous media: influence of ionic strength and pore velocity. *J Contam Hydrol* 2001;49:1–21.
- [27] Coston JA, Fuller CC, Davis JA. *Geochim Cosmochim Acta* 1995;59:3535–47.
- [28] Cumbie DH, McKay LD. Influence of diameter on article transport in a fractured shale saprolite. *J Contam Hydrol* 1999;37:139–57.
- [29] Cushing RS, Lawler DF. Depth filtration: fundamental investigation through three dimensional trajectory analysis. *Environ Sci Technol* 1998;32(23):3793–801.
- [30] Dabros T, van de Ven TGM. Particle deposition on partially coated surfaces. *Colloids Surf A: Physicochem Eng Aspects* 1993;75:95–104.
- [31] Dabros T. Interparticle hydrodynamic interactions in deposition processes. *Colloids Surf A: Physicochem Eng Aspects* 1989;39:127–41.
- [32] Dabros T, van de Ven TGM. Hydrodynamic interactions between two spheres near a solid plane. *Int J Multiphase Flow* 1992;18:751–64.
- [33] Das SK, Sharma MM, Schechter RS. Adhesion and removal of colloidal particles from surfaces. *Part Sci Technol* 1995;13:227–47.
- [34] Das SK, Schechter RS, Sharma MM. The role of surface roughness and contact deformation on the hydrodynamic detachment of particles from surfaces. *J Colloid Interface Sci* 1994;164:63–77.
- [35] Davis JA. Adsorption of dissolved natural organic matter at the oxide/water interface. *Geochim Cosmochim Acta* 1982;46:2381–93.
- [36] DeBorde DC, Woessner WW, Kiley QT, Ball P. Rapid transport of viruses in a floodplain aquifer. *Water Res* 1999;33(10):2229–38.
- [37] Deflaun MF, Murray CJ, Holben W, Scheibe T, Mills A, Ginn T. *FEMS Microbiol Rev* 1997;20:473–87.
- [38] Derjaguin BV, Landau L. *Acta Physicochim SSSR* 1941;14:633.
- [39] Ducker WA, Senden TJ, Pashley RM. Direct measurement of colloidal forces using an atomic force microscope. *Nature* 1991;353:239–41.
- [40] Elimelech M. Particle deposition on ideal collectors from dilute flowing suspensions: mathematical formulation, numerical solution, and simulations. *Sep Sci Technol* 1994;4(10):189–212.
- [41] Elimelech M, O’Melia CR. Kinetics of deposition of colloidal particles in porous media. *Environ Sci Technol* 1990;24:1528–36.
- [42] Elimelech M, Chen JY, Kuznar ZA. *Langmuir* 2003;19:6594.
- [43] Feick JD, Velegol D. Measurements of charge nonuniformity on polystyrene latex particles. *Langmuir* 2002;18:3454–8.
- [44] Fontes DE, Mills AL, Hornberger GM, Herman JS. Physical and chemical factors influencing transport of microorganisms through porous media. *Appl Environ Microbiol* 1991;57:2473–81.
- [45] Goldman AJ, Cox RG, Brenner H. Slow viscous motion of a sphere parallel to a plane wall – II. Couette flow. *Chem Eng Sci* 1967;22:653–60.
- [46] Grasso D, Smets BF, Strevett KA, Machinist BD, van Oss CJ, Giese RF, et al. Impact of physiological state on surface thermodynamics and adhesion of *Pseudomonas aeruginosa*. *Environ Sci Technol* 1996;30:3604–8.
- [47] Gregory J. Interaction of unequal double layer at constant charge. *J Colloid Interface Sci* 1975;51:44–51.
- [48] Gregory J. Approximate expression for retarded van der Waals interaction. *J Colloid Interface Sci* 1981;83:138–45.
- [49] Grolimund D, Borkovec M. Long-term release kinetics of colloidal particles from natural porous media. *Environ Sci Technol* 1999;33(2):4054–60.
- [50] Grolimund D, Barmettler K, Borkovec M. Release and transport of colloidal particles in natural porous media 2. Experimental results and effects of ligands. *Water Resour Res* 2001;37(3):571–82.
- [51] Hahn MW, Abadzic D, O’Melia CR. On the role of secondary minima. *Environ Sci Technol* 2004;38(22):5915–24.
- [52] Hahn MW, O’Melia CR. Deposition and reentrainment of Brownian particles in porous media under unfavorable chemical conditions: some concepts and applications. *Environ Sci Technol* 2004;38(1):210–20.
- [53] Harter T, Wagner S, Atwill ER. Colloid transport and filtration of cryptosporidium parvum in sandy soils and aquifer sediments. *Environ Sci Technol* 2000;34(1):62–70.
- [54] Hartley PG, Larson I, Scales PJ. Electrokinetic and direct force measurements between silica and mica surfaces in dilute electrolyte solutions. *Langmuir* 1997;13:2207–14.
- [55] Harvey RW, Kinner NE, Bunn A, MacDonald D, Metge DW. Transport behavior of groundwater protozoa and protozoan-sized microspheres in sandy aquifer sediments/. *Appl Environ Microb* 1995;61(1):209–17.
- [56] Harvey RW, Kinner NE, MacDonald D, Metge DW, Bunn A. Role of physical heterogeneity in the interpretation of small-scale laboratory and field observations of bacteria, microbial-sized microsphere, and bromide transport through aquifer sediments. *Water Resour Res* 1993;29(8):2713–21.
- [57] Harvey RW, Garabedian SP. Use of colloid filtration theory in modeling movement of bacteria through a contaminated sandy aquifer. *Environ Sci Technol* 1991;25(1):178–85.
- [58] Hayashi H, Tsuneda S, Hirata A, Sasaki H. Soft particle analysis of bacterial cells and its interpretation of cell adhesion behaviors in terms of DLVO theory. *Colloids Surf B: Biointerfaces* 2001;22:149–57.
- [59] Hendry MJ, Lawrence JR, Maloszewski P. Effects of velocity on the transport of two bacteria through saturated sand. *Groundwater* 1999;37(1):103–12.
- [60] Hodges CS, Cleaver JAS, Ghadiri M, Jones R, Pollock HM. Forces between polystyrene particles in water using the AFM: pull-off force vs particle size. *Langmuir* 2002;18:5741–8.

- [61] Hornberger GM, Mills AL, Herman JS. Bacterial transport in porous media: evaluation of a model using laboratory observations. *Water Resour Res* 1992;28:915–38.
- [62] Hubbe MA. Detachment of colloidal hydrous oxide spheres from flat solids exposed flow. 2. Mechanism of release. *Colloids Surf* 1985;16:249–70.
- [63] Israelachvili JN. Intermolecular and surface forces. 2nd ed. London: Academic Press; 1992.
- [64] Johnson PR, Sun N, Elimelech M. Colloid transport in geochemically heterogeneous porous media: modeling and measurements. *Environ Sci Technol* 1996;30(11):3284–93.
- [65] Johnson WP, Zhang P, Gardner PM, Fuller ME, DeFlaun MF. Monitoring the response of indigenous bacteria to the arrival of injected bacteria using ferrographic capture. *Appl Environ Microb* 2001;67(10):4908–13.
- [66] Johnson WP, Tong M, Li X. Colloid deposition in environmental porous media: deviation from existing theory is the norm; not the exception. *EOS* 2005;86(18):179–80.
- [67] Johnson WP, McIntosh WO. Field investigation of enhanced detachment of attached bacterial cells by hydrodynamic collision with injected bacteria. *J Microb Meth* 2003;1789:1–12.
- [68] Johnson WP, Blue KA, Logan BE, Arnold RG. Modeling bacterial detachment during transport through porous media as a residence-time-dependent process. *Water Resour Res* 1995;31(11):2649–58.
- [69] Johnson WP, Li X. Comment on: Tufenkji and Elimelech (2005) Breakdown of colloid filtration theory: role of the secondary energy minimum and surface charge heterogeneities. *Langmuir* 2005;21:841–52. 10895–10895.
- [70] Johnson KL. Contact mechanics. 1st ed. Cambridge, UK: Cambridge University Press; 1985.
- [71] Johnson KL, Kendall K, Roberts AD. Surface energy and the contact of elastic solids. *Proc R Soc Lond A* 1971;324:301–13.
- [72] Jones JF, Feick JD, Imoudu D, Chukwumah N, Vigeant M, Velegol D. Oriented adhesion of *Escherichia coli* to polystyrene particles. *Appl Environ Microb* 2003;69(11):6515–9.
- [73] Jucker BA, Zehnder AJB, Harms H. Quantification of polymer interactions in bacterial adhesion. *Environ Sci Technol* 1998;32:2909–15.
- [74] Jucker BA, Harms H, Hug SJ, Zehnder AJB. Adsorption of bacterial surface polysaccharides on mineral oxides is mediated by hydrogen bonds. *Colloids Surf B: Biointerfaces* 1997;9:331–43.
- [75] Kallay N, Tomić M, Biškup B, Kunjašić I, Matejević E. Particle adhesion and removal in model system. XI. Kinetics of attachment and detachment for hematite–glass systems. *Colloids Surf* 1987;28:185–97.
- [76] Keller AA, Sirivithapakorn S, Chrysikopoulos CV. Early breakthrough of colloids and bacteriophage MS2 in a water-saturated sand column. *Water Resour Res* 2004;40:W08304. doi:10.1029/2003WR00267.
- [77] Ko C, Elimelech M. The “shadow effect” in colloid transport and deposition dynamics in granular porous media: measurements and mechanisms. *Environ Sci Technol* 2000;34:3681–9.
- [78] Kretzschmar R, Barmettler K, Grolimund D, Yan Y, Borkovec M, Sticher H. Experimental determination of colloid deposition rates and collision efficiencies in natural porous media. *Water Resour Res* 1997;33:1129–37.
- [79] Li Q, Logan BE. Enhancing bacterial transport for bioaugmentation of aquifers using low ionic strength solutions and surfactants. *Water Res* 1999;33(4):1090–100.
- [80] Li X, Johnson WP. Non-monotonic variations in removal rate coefficients of microspheres in porous media under unfavorable deposition conditions. *Environ Sci Technol* 2005;39:1658–65.
- [81] Li X, Scheibe TD, Johnson WP. Apparent decreases in colloid removal rate coefficients with distance of transport under unfavorable deposition conditions: a general phenomenon. *Environ Sci Technol* 2004;38(21):5616–25.
- [82] Lindqvist R, Cho JS, Enfield CG. A kinetic model for cell density dependent bacterial transport in porous media. *Water Resour Res* 1994;30:3291–9.
- [83] Logan BE, Jewett DJ, Arnold RG, Bouwer EJ, O’Melia CR. *J Environ Eng* 1995;121:869–73.
- [84] McCarthy JF. Colloid transport and mobilization in subsurface environments, Preprints of extended abstracts, 217th ACS national meeting, Anaheim, CA, March 21–25, vol. 39(1), 1999. p. 270–1.
- [85] McCaulou DR, Bales RC, Arnold RG. Effect of temperature controlled motility on transport of bacteria and microspheres through saturated sediment. *Water Resour Res* 1995;31:271–80.
- [86] Meinders JM, Busscher HJ. Adsorption and desorption of colloidal particles on glass in a parallel plate flow chamber – influence of ionic strength and shear rate. *Colloid Polym Sci* 1994;272:478–86.
- [87] Meinders JM, Busscher HJ. Influence of interparticle interactions on blocked areas and desorption during particle deposition to glass in a parallel plate flow chamber. *Langmuir* 1995;11:327–33.
- [88] Meinders JM, Noordmans J, Busscher HJ. Simultaneous monitoring of the adsorption and desorption of colloidal particles during deposition in a parallel plate flow chamber. *J Colloid Interface Sci* 1992;152(1):265–80.
- [89] Meinders JM, van der Mei HC, Busscher HJ. Deposition efficiency and reversibility of bacterial adhesion under flow. *J Colloid Interface Sci* 1995;176:329–41.
- [90] Morisaki H, Nagai S, Oshima H, Ikemoto E, Kogoe K. The effect of motility and cell-surface polymers on bacterial attachment. *Microbiology* 1999;145:2797–802.
- [91] Morley LM, Hornberger GM, Mills AL, Herman JS. Effects of transverse mixing on transport of bacteria through heterogeneous porous media. *Water Resour Res* 1998;34(8):1901–8.
- [92] Murphy EM, Ginn TR. Modeling microbial processes in porous media. *Hydrogeol J* 2000;8:142–58.
- [93] Nelson KE, Ginn TR. Colloid filtration theory and the Happel sphere-in-cell model revisited with direct numerical simulation of colloids. *Langmuir* 2005;21(6):2173–84.
- [94] Neu TR. Significance of bacterial surface active compounds in interaction of bacteria with interfaces. *Microb Rev* 1996;60:151.
- [95] Niehren S, Kinzelbach W. Artificial colloid tracer tests: development of a compact on-line microsphere counter and application to soil column experiments. *J Contam Hydrol* 1998;36:249–59.
- [96] O’Neill MN. A sphere in contact with a plane wall in a slow linear shear flow. *Chem Eng Sci* 1968;23:1293–8.
- [97] Ong YL, Razatos A, Georgiou G, Sharma MM. Adhesion forces between *E. coli* bacteria and biomaterial surfaces. *Langmuir* 1999;15:2719–25.
- [98] Oshima H. Electrophoretic mobility of soft particles. *J Colloid Interface Sci* 1994;163:474–83.
- [99] Oshima H. Electrophoretic mobility of soft particles. *Colloids Surf A: Physicochem Eng Aspects* 1995;103:249–55.
- [100] Pang L, Close M, Goltz M, Noonan M, Sinton L. Filtration and transport of *Bacillus subtilis* spores and the F-RNA phage MS2 in a coarse alluvial gravel aquifer: implications in the estimation of setback distances. *J Contam Hydrol* 2005;77:165–94.
- [101] Pang L, Close M, Noonan M. Rhodamine WT and *Bacillus subtilis* transport through an alluvial gravel aquifer. *Ground Water* 1998;36(1):112–22.
- [102] Payatakes AC, Tien C, Turian RM. A new model for granular porous media. *AIChE J* 1973;19(1):58–67.
- [103] Pieper AP, Ryan JN, Harvey RW, Amy GL, Illangasekare TH, Metge DW. *Environ Sci Technol* 1997;31(4):1163–70.
- [104] Prieve DC, Lin MMJ. Adsorption of Brownian hydrosols onto a rotating disc aided by a uniform applied force. *J Colloid Interface Sci* 1979;76:32–47.
- [105] Rajgopalan R, Tien C. Trajectory analysis of deep-bed filtration with the sphere-in-cell porous media model. *AIChE J* 1976;22(3):523–33.
- [106] Redman JA, Estes MK, Grant SB. Resolving macroscale and microscale heterogeneity in pathogen filtration. *Colloids Surf A: Physicochem Eng Aspects* 2001;191(1–2):57–70.

- [107] Redman JA, Walker SL, Elimelech M. Bacterial adhesion and transport in porous media: role of the secondary energy minimum. *Environ Sci Technol* 2004;38(6):1777–85.
- [108] Rinjaarts HHM, Norde W, Bouwer EJ, Lyklema J, Zehnder AJB. Bacterial deposition in porous media related to the clean bed collision efficiency and substratum blocking by attached cells. *Environ Sci Technol* 1996;30(10):2869–76.
- [109] Ryan JN, Gschwend PM. Effect of solution chemistry on clay colloid release from an iron oxide-coated aquifer sand. *Environ Sci Technol* 1994;28:1717–26.
- [110] Ryan JN, Gschwend PM. Effects of ionic strength and flow rate on colloid release: relating kinetics to intersurface potential energy. *J Colloid Interface Sci* 1994;164:21–34.
- [111] Ryan JN, Elimelech M, Ard RA, Harvey RW, Johnson PR. Bacteriophage PRD1 and silica colloid transport in an iron oxide-coated sand aquifer. *Environ Sci Technol* 1999;33(1):63–73.
- [112] Ryan JN, Elimelech M. Colloid mobilization and transport in groundwater. *Colloids Surf A: Physicochem Eng Aspects* 1996;107:1–56.
- [113] Sader JE, Chon JWM, Mulvaney P. Calibration of rectangular atomic force microscope cantilevers. *Rev Sci Instrum* 1999;70(10):3967–9.
- [114] Sakthivadivel R. Rep. HEL15-7, Hydr. Eng. Lab., University of California, Berkeley, 1969.
- [115] Scheibe TD, Wood BD. A particle-based model of size or anion exclusion with application to microbial transport in porous media. *Water Resour Res* 2003;39(4). doi:10.1029/2001WR00122.
- [116] Schijven JF, Hoogenboezem W, Hassanizadeh SM, Peters JH. Modeling removal of bacteriophages MS2 and PRD1 by dune filtration at Castricum, the Netherlands. *Water Resour Res* 1999;35:1101–11.
- [117] Scholl MA, Harvey RW. Laboratory investigations on the role of sediment surface and groundwater chemistry on the transport of bacteria through a contaminated sandy aquifer. *Environ Sci Technol* 1992;26:1410–7.
- [118] Sharma MM, Chamoun H, Sita Rama Sarma DSH, Schechter RS. Factors controlling the hydrodynamic detachment of particles from surfaces. *J Colloid Interface Sci* 1992;149:121–34.
- [119] Shellenberger K, Logan BE. Effect of molecular scale roughness of glass beads on colloidal and bacterial deposition. *Environ Sci Technol* 2002;36(2):184–9.
- [120] Simoni SF, Harms H, Bosma TNP, Zehnder AJB. *Environ Sci Technol* 1998;32:2100–5.
- [121] von Smoluchowski M. Versuch einer mathematischen theorie der koagulationskinetik kolloider lösungen. *Z Phys Chem* 1918;92:129–68.
- [122] Song L, Elimelech M. Dynamics of colloid deposition in porous media: modeling the role of retained particles. *Colloids Surf A: Physicochem Eng Aspects* 1993;73:49–63.
- [123] Song L, Elimelech M. Transient deposition of colloidal particles in heterogeneous porous media. *J Colloid Interface Sci* 1994;167:301–13.
- [124] Tan S, Sherman RL, Qin D, Ford WT. Surface heterogeneity of polystyrene latex particles determined by dynamic force microscopy. *Langmuir* 2005;21:43–9.
- [125] Tan Y, Gannon JT, Baveye P, Alexander M. Transport of bacteria in aquifer sand: experiments and model simulations. *Water Resour Res* 1994;30(12):3243–52.
- [126] Thurman EM. *Organic Geochemistry of Natural Waters*. Dordrecht, The Netherlands: Martinus Nijhoff/Junk; 1985.
- [127] Tipping E, Cooke D. The effects of adsorbed humic substances on the surface charge of goethite in freshwaters. *Geochim Cosmochim Acta* 1982;46:75–80.
- [128] Tong M, Camesano TA, Johnson WP. Spatial variation in deposition rate coefficients of an adhesion deficient bacterial strain in quartz sand. *Environ Sci Technol* 2005;39(10):3679–87.
- [129] Tong M, Li X, Brow C, Johnson WP. Detachment-influenced transport of an adhesion-deficient bacterial strain in water-reactive porous media. *Environ Sci Technol* 2005;39(8):2500–8.
- [130] Toran L, Palumbo AV. Colloid transport through fractured and unfractured laboratory sand columns. *J Contam Hydrol* 1992;9:289–303.
- [131] Tufenkji N, Elimelech M. Correlation equation for predicting single-collector efficiency in physicochemical filtration in saturated porous media. *Environ Sci Technol* 2004;38(2):529–36.
- [132] Tufenkji N, Elimelech M. Deviation from classical colloid filtration theory in the presence of repulsive DLVO interactions. *Langmuir* 2004;20(25):10818–28.
- [133] Tufenkji N, Miller GF, Ryan J, Harvey RW, Elimelech M. Transport of cryptosporidium oocysts in porous media: role of straining and physicochemical filtration. *Environ Sci Technol* 2004;38(22):5932–8.
- [134] Tufenkji N, Elimelech M. Breakdown of colloid filtration theory: role of secondary energy minimum and surface charge heterogeneities. *Langmuir* 2005;21:841–52.
- [135] Tufenkji N, Elimelech M. Response to Comment on: Tufenkji and Elimelech (2005) Breakdown of colloid filtration theory: role of the secondary energy minimum and surface charge heterogeneities. *Langmuir* 2005;21:841–52. 10896–7.
- [136] van Oss CJ. *J Colloids Surf B* 1995;5:91–110.
- [137] van Oss CJ. *Interfacial forces in aqueous media*. 1st ed. New York: Marcel Dekker; 1994.
- [138] Varennes S, van de Ven TGM. Deposition and detachment of latex particles at glass surfaces exposed to flow. *Phys Chem Hydrodyn* 1987;9:537–59.
- [139] Veeramasoneni S, Yalamanchili MR, Miller JD. Measurement of interaction forces between silica and α -alumina by atomic force microscopy. *J Colloid Interface Sci* 1996;184:594–600.
- [140] Veeramasoneni S, Yalamanchili MR, Miller JD. Interactions between dissimilar surfaces in high ionic strength solutions as determined by atomic force microscopy. *Colloids Surf A: Physicochem Eng Aspects* 1998;131:77–88.
- [141] Velegol SB, Logan BE. Contributions of bacterial surface polymers, electrostatics, and cell elasticity to the shape of AFM force curves. *Langmuir* 2002;18:5256–62.
- [142] Verwey EJW, Overbeek JThG. *Theory of the stability of lyophobic colloids*. Amsterdam: Elsevier; 1948.
- [143] Vigeant MAS, Ford RM. Interactions between motile *Escherichia coli* and glass in media with various ionic strengths, as observed with a three-dimensional tracking microscope. *Appl Environ Microb* 1997;63(9):3474–9.
- [144] Vigeant MAS, Ford RM, Wagner M, Tamm LK. Reversible and irreversible adhesion of motile *Escherichia coli* cells analyzed by total internal reflection aqueous fluorescence microscopy. *Appl Environ Microb* 2002;68(6):2794–801.
- [145] Vilks P, Bachinski DB. Colloid and suspended particle migration experiments in a granite fracture. *J Contam Hydrol* 1996;21:269–79.
- [146] Visser J. In: Matijević E, editor. *Surface and colloid science*. New York: Wiley; 1976.
- [147] Walker SL, Redman JA, Elimelech M. Role of cell surface lipopolysaccharides (LPS) in *Escherichia coli* K12 adhesion and transport. *Langmuir* 2004;20(18):7736–46.
- [148] Weiss M, Luthi Y, Rička J. Colloidal particles at solid-liquid interfaces: mechanisms of desorption kinetics. *J Colloid Interface Sci* 1998;206:322–31.
- [149] Yan YD. Pulse-injection chromatographic determination of the deposition and release rate constants of colloidal particles in porous media. *Langmuir* 1996;12:3383–8.
- [150] Yang C, Dabros T, Li D, Czarnecki J, Masliyah JH. Kinetics of particle transport to a solid surface from an impinging jet under surface and external force fields. *J Colloid Interface Sci* 1998;208: 226–40.
- [151] Yao KM, Habibian MT, O'Melia CR. *Water and waste water filtration: concepts and applications*. *Environ Sci Technol* 1971;5: 1105–12.
- [152] Yiantsios SG, Karabelas AJ. Detachment of spherical microsparticles adhering on flat surfaces by hydrodynamic forces. *J Colloid Interface Sci* 1995;176:74–85.

[153] Zhang PF, Johnson WP, Scheibe TD, Choi Keun-Hyung, Dobbs FC, Mailloux BJ. Extended tailing of bacterial following breakthrough at the Narrow Channel focus area, Oyster, Virginia. *Water Resour Res* 2001;37:2687–98.

[154] Zhang PF, Johnson WP, Piana MJ, Fuller CC, Naftz DL. Potential artifacts in interpretation of differential breakthrough of colloids and dissolved tracers in the context of transport in a zero-valent iron permeable reactive barrier. *Ground Water* 2001;39:831–40.

Author's personal copy